Mucosal Immunology xxx (xxxx) xxx

Contents lists available at ScienceDirect

Mucosal Immunology

journal homepage: www.elsevier.com/mi

Distal airway epithelial progenitors mediate TGF-β release to drive lung CD8$^+$ T_{RM} induction following mucosal BCG vaccination

Judith A. Blake [a], Julia Seifert [a], Socorro Miranda-Hernandez [a], Roland Ruscher [a], Paul R. Giacomin [a], Denise L. Doolan [a,b], Andreas Kupz [a,*]

[a] Australian Institute of Tropical Health and Medicine, James Cook University, Cairns, Australia
[b] Institute for Molecular Bioscience, University of Queensland, Brisbane, Australia

ARTICLE INFO

Keywords:
BCG
Tuberculosis
TGF-β
Mucosal
Airway epithelial progenitors
Resident memory T cells

ABSTRACT

A principal reason for the high global morbidity and mortality of tuberculosis (TB) is the lack of efficacy of the only licensed TB vaccine, Bacillus Calmette-Guérin (BCG), as intradermal BCG does not induce local pulmonary immune memory. Animal studies have shown that inhalation of BCG vaccination provides superior mucosal protection against TB due to generation of lung resident memory T cells (T_{RM}). Here, we demonstrated that following mucosal vaccination with the genetically modified more virulent BCG strain, BCG::RD1, distal airway epithelial progenitors were mobilized to assist with restoration of alveolar epithelium. By way of their integrin-mediated activation of latent TGF-β, lung CD8$^+$ T_{RM} differentiation was induced. Mucosal vaccinations using nonvirulent strains of BCG in which airway epithelial progenitors were not mobilized, as well as genetic inhibition of integrin-mediated activation of TGF-β, resulted in significantly lower numbers of lung CD8$^+$ T_{RM} with subsequent reduced protection against *Mycobacterium tuberculosis* (*Mtb*)-induced lung pathology in mice. The results link airway epithelial progenitor-mediated repair of injured lung tissue with a role in the induction of resident CD8$^+$ T cell memory. These findings provide further explanation why mucosal vaccination with virulent BCG strains is more protective against TB and thus has implications for future TB vaccine development.

Introduction

During the Covid-19 pandemic, the ineffectiveness of a non-mucosal vaccine to protect against lung infection became more apparent, a problem well acknowledged amongst TB immunologists.[1] TB is primarily a respiratory infection caused by *Mycobacterium tuberculosis* (*Mtb*; with 10.8 million new infections in 2023 and 1.25 million deaths, TB is one of the top ten fatal diseases globally.[2] These statistics highlight the inadequacy of the only licensed TB vaccine – BCG.[1,3,4] BCG is an attenuated strain of *Mycobacterium bovis* given to postnatal infants in TB endemic regions to confer immunity against septic forms of TB,[5] however, immunity is often lost in adolescence.[6] Failure of BCG to provide life-long immunity against *Mtb* is a motivation for vaccine improvement where recombinant modifications of BCG aim to generate a more persistent T cell memory. For example, mice and guinea pigs vaccinated with BCG strains in which the region of difference 1 (RD1) genes that encode *Mtb* virulence genes ESAT-6 and CFP-10 were recombined into *M. bovis* BCG (BCG::RD1)[7] showed improved protection against *Mtb* challenge.[8,9]

It has also been demonstrated that mucosal BCG vaccination, as opposed to subcutaneous (SC) or intradermal BCG, generated superior protection against TB in animal models and this protection was linked to generation of lung T_{RM} (subcutaneous/intradermal BCG did not lead to T_{RM} in the lungs).[8,10] Mucosal delivery of BCG::RD1 has been further shown to induce significant increases of airway T_{RM}[11] and conferred superior immunity against aerosol *Mtb* infection in diabetic mice.[12] Thus, immunogenic antigens of BCG::RD1[8] combined with a mucosal delivery strongly contributes to vaccine-induced protection against *Mtb*.

Abbreviations: AEC, alveolar epithelial cell; AEP, alveolar epithelial progenitor; BCG, Bacillus Calmette-Guérin; CFU, colony forming unit; DASC, distal airway stem cell; GFP, green fluorescent protein; *ItgB6*, integrin beta-6; IT, intratracheal; LNEP, lineage negative epithelial progenitor; mLN, mediastinal lymph node; *Mtb*, *Mycobacterium tuberculosis*; pSPC, pro-surfactant protein C; RAMD, repair-associated memory depot; RD1, region of difference 1; CD3 epsilon (CD3e), RFP, red fluorescent protein; SC, subcutaneous; T1α, type 1 alpha protein; TB, tuberculosis; TGF-β, transforming growth factor beta; T_{RM}, resident memory T cell.

* Corresponding author at: James Cook University, AITHM, McGregor Road, Building E5, Smithfield/ Cairns, Queensland 4878, Australia.
E-mail addresses: judith.blake@my.jcu.edu.au (J.A. Blake), julia.seifert@jcu.edu.au (J. Seifert), socorro.mirandahernandez1@jcu.edu.au (S. Miranda-Hernandez), roland.ruscher@jcu.edu.au (R. Ruscher), paul.giacomin@jcu.edu.au (P.R. Giacomin), d.doolan@imb.uq.edu.au (D.L. Doolan), andreas.kupz@jcu.edu.au (A. Kupz).

https://doi.org/10.1016/j.mucimm.2025.05.007
Received 5 March 2025; Accepted 26 May 2025
Available online 30 May 2025

How BCG virulence, T_{RM} induction and protection against TB are mechanistically linked remained elusive.

Evidence of interaction between immune and progenitor cells is seen in the array of immune receptors and cytokine signalling systems of progenitor cells[13–15] and dysregulation of immune-progenitor cell interactions that result in chronic disease.[16–18] In mouse models of acute influenza infection, there is an invariable association of $CD8^+$ T_{RM} and lung epithelial progenitor cells in areas of severe tissue destruction[19–26] and it has been suggested that "auxiliary developed regenerative tissues could be a source of unique factors necessary for differentiation and maintenance of T_{RM} cells, such as TGF-β".[27]

Lung injury activates epithelial progenitors to regenerate the alveolar epithelium which consists of Type 1 and Type 2 alveolar epithelial cells (AEC1 and AEC2, respectively). AEC1 are responsible for gas exchange while AEC2 secrete surfactant to prevent alveolar collapse, amongst many other functions, including the capacity to act as progenitors for excessive losses of AEC1.[28] A rare AEC progenitor (AEP) that constitutes ~20 % of all AEC2 has also been described.[22,29] Although stem cells, AEP express AEC2 markers including the precursor form of surfactant protein C (pSPC) and function as AEC2 but have a distinct gene expression profile enriched in lung developmental genes and epigenome.[22] Thus, both AEC2 and AEP progenitors express and are labelled by pSPC and here are collectively referred to as $pSPC^+$ alveolar epithelial progenitors.

Following severe depletion of normally abundant local $pSPC^+$ alveolar epithelial progenitor cells, stem cell responses originate from the airways.[30] The SRY-box 2 (SOX2) transcription factor is expressed in most airway epithelial cells of the adult mouse lung.[30] Of relevance to our studies are distal airway $Sox2^+$ lineage positive and lineage negative epithelial progenitors (here, collectively referred to as Sox^+ distal airway progenitors) and cytokeratin 5 ($Krt5^+$) distal airway stem cells (DASC). $Sox2^+$ distal airway progenitors are quiescent in uninjured lungs, however, alveolar injury elicits their proliferation, such that daughter cells migrate into alveolar tissue and differentiate into AEC1 or AEC2.[31,32] When $Sox2^+$ distal airway progenitors are lost (such as after murine PR8 influenza virus)[33]rare, quiescent DASC proliferate, and daughters migrate to occupy alveolar areas depleted of epithelium where they form $Krt5^+$ "pods" with $CD8^+$ T_{RM}[21,34] in a structure that has been termed a repair-associated memory depot (RAMD).[34] "

Finally, a novel distinct transitional progenitor cell population that expresses cytokeratin 8 (Krt8) has also been described by several groups that is relevant to this project. These $Krt8^+$ progenitors represent an intermediate cell state in which both cuboidal $pSPC^+$ alveolar and $Sox2^+$ airway progenitor cells convert physically, structurally, and mechanically into squamous AEC1 that function for gas-exchange.[32,35,36]

Before this research, regulation of $CD8^+$ T_{RM} induction and maintenance following mucosal exposure to mycobacteria and coregulation by epithelial progenitors, remained unknown; therefore, we sought to elucidate how they cooperate for restoration of lung function following mucosal BCG vaccination. Here, we describe a novel mechanistic association between distal airway epithelial progenitor paracrine cues and induction of protective $CD8^+$ lung $T_{RM.}$

Materials and methods

Animals

Female mice were 6–8 weeks old at the time of vaccination (female mice show a more robust humoral and cellular immunity after pulmonary infection)[37,38] and maintained in a biosafety level 2 facility under specific pathogen free conditions. C57BL/6 mice (ARC, Western Australia), *Krt5*^{CreERT2} mice (provided by Dr Felicity Davis, University of Queensland), *Axin2*$^{CreERT2:TdT}$*/EYFP* mice (provided by Dr Edward Morrisey, University of Pennsylvania), *Sox2*^{CreERT2} (Jackson Laboratories), *Itgβ6* knockout mice (provided by Dr Dean Sheppard, University of California San Francisco), *B6.Cg-Gt(ROSA)26Sor*$^{tm14(CAG-tdTomato)Hze}$*/J* mice (provided by Dr Scott Mueller, University of Melbourne), *Gt (ROSA)26Sor*$^{tm4(ACTB-tdTomato,-EGFP)Luo}$*/J* mice originally from Jackson Laboratories with substrain donated by Dr Scott Mueller (University of Melbourne) were all genotyped by Genetic Research Services (University of Queensland), bred and maintained in the animal facilities at James Cook University, Australia. The study (A2837) was approved by the James Cook University Animal Ethics Committee.

Bacteria

BCG SSI (ATCC no. 35733) and BCG::RD1 (provided by Dr Roland Brosch, Institut Pasteur) were grown in Middlebrook 7H9 broth (BD Biosciences) supplemented with 0.2 % glycerol, 0.05 % Tween 80, and 10 % ADC enrichment (BD Biosciences) as previously described.[12]

Mucosal immunisation and infection

Mice were immunized by IT instillation of 1×10^5 or 5×10^5 colony forming units (CFU) of BCG diluted in sterile PBS as described previously.[10] To determine vaccine protective efficacy, mice were challenged via the aerosol route with 50–100 CFU of *M. tuberculosis* H37Rv 60 days post vaccination by using a Glas-Col inhalation exposure system. Animals were monitored on a weekly basis, with determination of weight and scoring of body condition using the mouse BCS scale. At the doses utilized in this study, none of the animals met institutional animal care and use committee approved endpoints and they were analysed at the planned time-points.

Lung inflation

After euthanasia by CO_2 inhalation, animals were exsanguinated; the thorax was opened to expose the lungs. Lungs were inflated via trachea with 0.5 % zinc acetate and zinc chloride in 0.5 % tris-calcium acetate buffer (ZBF; BD Biosciences) at a fluid pressure of 25 cm before removal *en bloc* and incubation in 30 ml ZBF at 25°C for 72 hr prior to 24-hr incubation at 25°C in 50 % ethanol.

Immunohistochemistry

Fixed tissues were dehydrated with an automated tissue processor (Leica Biosystems) and embedded in paraffin blocks, 4 μm sections cut and collected on Polysine slides (ProSciTech), dried at 25°C overnight prior to deparaffinization using standard protocols. H&E staining was performed using an automated processor (Leica Biosystems). Sections were washed with Tris-buffered saline (TBS) and blocked with 10 % species-specific serum to secondary antibodies at 25°C for 2 hr. Primary antibodies were incubated overnight at 4°C (Supp. Table 1). Tissues were incubated with peroxidase inhibitor (Thermo Fisher Scientific) for 30 min at 25°C. For avidin biotin complex (ABC) IHC, endogenous avidin binding activity was quenched with avidin and biotin blocking buffers (Abcam) for 15 min at 25°C, before incubation with secondary antibodies for 1 hr at 25°C in optimized dilutions (Supp. Table 1). For ABC IHC, tissue incubated with 45 μl of Vectastain ABC kit reagents (Vector Laboratories) in 10 ml TBS for 30 min at 25°C. Tissue was washed before incubation with DAB chromogen (Abcam) for 3–5 min, and counterstained with hematoxylin (Sigma-Aldrich). Tissues were cleared using standard protocols and cover slipped with Surgipath mounting media (Leica) and #1 coverslips (Leica).

Microscopy

Images were acquired using an Aperio CS2 Digital Slide Scanner (Leica Biosystems) and analyzed using Aperio ImageScope v12.4.3.5008 software (Leica Biosystems). Quantification of $Krt8^+$ TP, active TGF-β and Sox2 lineage traced RFP^+ cells was undertaken using ImageJ software (ImageJ).

Lung and mediastinal lymph node dissociation

Lung and spleen dissociation kits (Miltenyi Biotec) were used to dissociate lung and mLN into single cell suspensions according to manufacturer's instructions. After the final dissociation step, supernatant was aspirated before addition of 3 ml RBC lysis buffer (Thermo Fisher Scientific), resuspension and incubation for 2 min. 10 ml FACS buffer was added prior to centrifugation at 1500 rpm for 5 min at 25°C. Supernatant was discarded and cells resuspended with FACS buffer to 500 µl.

Flow cytometry and data analyses

150 µl of dissociated cells were pipetted into 96 round bottom well plate and spun at 1500 rpm at 4°C for 5 min. Cells were resuspended in 50 µl Live/Dead cell stain 1:1000 (APC-Cy7 channel) (BD Biosciences) and incubated at 25°C for 10 min in the dark. Samples were washed with FACS buffer, spun at 1500 rpm for 5 min at 4°C. Samples were resuspended in 50 µl antibody master mix (Supp. Table 1) at optimized concentrations before incubation for 30 min on ice in the dark. After washes and spin at 1500 rpm at 4°C for 5 min, 150 µl Sphero Blank Calibration Particles (BD Biosciences) at 1:75 was added to resuspended samples. Flow cytometry analyses were performed on a LSR Fortessa X20 cytometer using FACSDiva software (BD Biosciences). The data were analysed by FlowJo software (Treestar).

Lineage tracing

A single dose of 0.125 mg/g body weight tamoxifen (Sigma-Aldrich) was dissolved in 50 µl corn oil (Sigma-Aldrich) and administered to $Krt5^{CreERT2}/mTmG$ mice intraperitoneally at day 14 after IT vaccination with BCG::RD1. Three doses of 0.25 mg/g tamoxifen was administered every second day to $Sox2^{CreERT2}/Ai14$ mice and every day for 5 days to $Axin2^{CreERT2:TdT}/EYFP$ mice 28 days prior to IT vaccinations. Tamoxifen-independent recombination in $Krt5^{CreERT2}/mTmG$ mice was 0% with no systemic effects in floxed littermate controls. In $Sox2^{CreERT2}/Ai14$ mice tamoxifen independent recombination was less than 1%, while floxed controls were negative for systemic effects. $Axin2^{CreERT2:TdT}/EYFP$ were unable to be analysed for independent recombination due to excessive lung pathology.

Statistical analysis

Statistical analysis and graphs were generated using Prism version 9.5.1 (GraphPad). Two parametric group analyses were carried out using Student's *t* test, followed by Holm-Šídák multiple comparison tests. Analyses of variance between independent groups were carried out using One-way ANOVA by Tukey's multiple comparison tests. $P < 0.05$ was considered significant.

Results

BCG virulence and dose affects loss of alveolar epithelial cells

We undertook an initial study of the responses of lung epithelial cells to mucosal vaccination with BCG strains across a spectrum of dose and virulence over time, using intratracheal (IT) vaccination of C57BL/6 mice (n = 6/time point) with the Danish strain of BCG (BCG SSI) at a dose of 100,000 colony forming units (CFU), BCG SSI at 500,000 CFU, BCG::RD1 at 100,000 CFU or PBS (Fig. 1a). AEC2 are frontline cells of mycobacterial invasion[39]; also, infection-related cytolysis of AEC2 affects AEC1 that are particularly sensitive to epithelial damage.[40] To determine the relative number of AEC lost (the impetus for immune and subsequent progenitor cell responses) across our vaccinations, lung sections were immunostained using type 1 alpha protein (T1α) and prosurfactant protein C (pSPC), before image analyses of AEC1 and AEC2 losses, respectively, across a four-month timeline. We combined descriptive analyses and semiquantitative scoring systems to evaluate different parameters associated with understanding the timeline of repercussions to the vaccinations.[41] Lung sections from each mouse (3 for each 2 experimental replicates; n = 6) across the 7–120 days after vaccination time span were graded for relative severity of pathology guided by the United States Department of Health and Human Services National Toxicology (Respiratory) Program.[42] Alveolar epithelial cell pathology was graded for distortion of normal tissue architecture, alveolar epithelial degeneration (evidenced by cell shrinkage and/or pykinosis), and/or alveolar epithelial necrosis (characterised by cell swelling, fragmentation, disrupted architecture, loss of staining intensity, and/or sloughing of necrotic cells/ debris into the alveolar or airway lumen). Compared to normal lung (Fig. 1b; Supp. Fig. 1a), AEC pathology (Fig. 1c; Supp. Fig. 1b) was graded as normal (Grade 0), minimal (Grade 1), moderate (Grade 2) or severe (Grade 3).

Following BCG SSI low dose vaccination, minimal AEC pathology was observed by the peak of injury at 21 days past vaccination (dpv) (Fig. 2a, b) AEC pathology consisted of alveolar wall hyperplasia and sparse small focal lesions (Supp. Fig. 2a, b). Following BCG SSI high dose vaccination, moderate AEC pathology was observed by the peak of injury at 21 dpv (Fig. 2a, b). AEC pathology consisted of global focal peribronchiolar lesions (Supp. Fig. 2c, d). After BCG::RD1 vaccination, a marked AEC pathology occurred by a peak at 21 dpv, (Fig. 2a, b). AEC pathology consisted of large global areas of severe destruction of both AEC visible by loss of staining intensity with necrosis evidenced by $T1\alpha^{+}$ cell debris in bronchiolar lumen (Supp. Fig. 2e, f). When we had established that the peak of tissue damage was 21 dpv following all vaccinations using semi-quantitative methods, we quantified AEC pathology (Fig. 2c, d) to demonstrate that dose and virulence of mucosal BCG vaccination were directly related to pathology.

BCG dose, virulence and delivery impacts lung inflammation and T cell influx

To broadly understand the inflammatory and CD3 T cell responses to AEC invasion and pathology, lung sections from each mouse (3 for each 2 experimental replicates; n = 6) across the 7–120 days after vaccination time span were stained with hematoxylin and eosin (H&E) and immunostained with CD3 epsilon (CD3e), before semi-quantitative grading of inflammation and T cell infiltration, respectively. Histological evidence of inflammation included parameters of infiltration of neutrophils, macrophages and leukocytes, aggregations of activated macrophages and/or multinucleated giant cells (Supp Fig. 3a, b), focal lesions (Supp. Fig. 3a), haemorrhage (accumulations of extravasated blood cells in alveolar lumina; Supp. Fig. 3a, c), and parenchymal cell damage caused by haemorrhage. Compared to normal lung (Supp. Fig. 3d), inflammatory pathology was graded as none (Grade 0), minimal (Grade 1), moderate (Grade 2) or marked (Grade 3). Histological evidence of CD3 infiltration (Supp. Fig. 4) was graded as none (Grade 0), minimal (Grade 1), moderate (Grade 2) or marked (Grade 3). With this work, we sought to gain an oversight of the time of the peak of tissue damage across the various vaccinations.

After BCG SSI low dose vaccination, inflammation rose slowly to peak at moderate levels by 21–28 dpv and largely resolved by 35 dpv (Fig. 2e) and T cells infiltrated reaching moderate numbers by 21 dpv and declining steadily thereafter (Fig. 2f). The inflammatory response consisted of small haemorrhagic lesions (Supp. Fig. 5a) due to vascular changes and minimal focal peribronchiolar and perivascular inflammation. When BCG SSI was administered at a high dose, inflammation, and T cell infiltration peaked at 21 dpv until 35 dpv (Fig. 2e, f). The inflammatory response consisted of global focal areas of haemorrhage due to capillary changes and moderate peribronchiolar and perivascular immune cell infiltrates (primarily T cells), as well as moderate numbers of interstitial giant cell macrophages (Supp. Fig. 5b). Following BCG::RD1 vaccination, global inflammation escalated to severe levels by 21

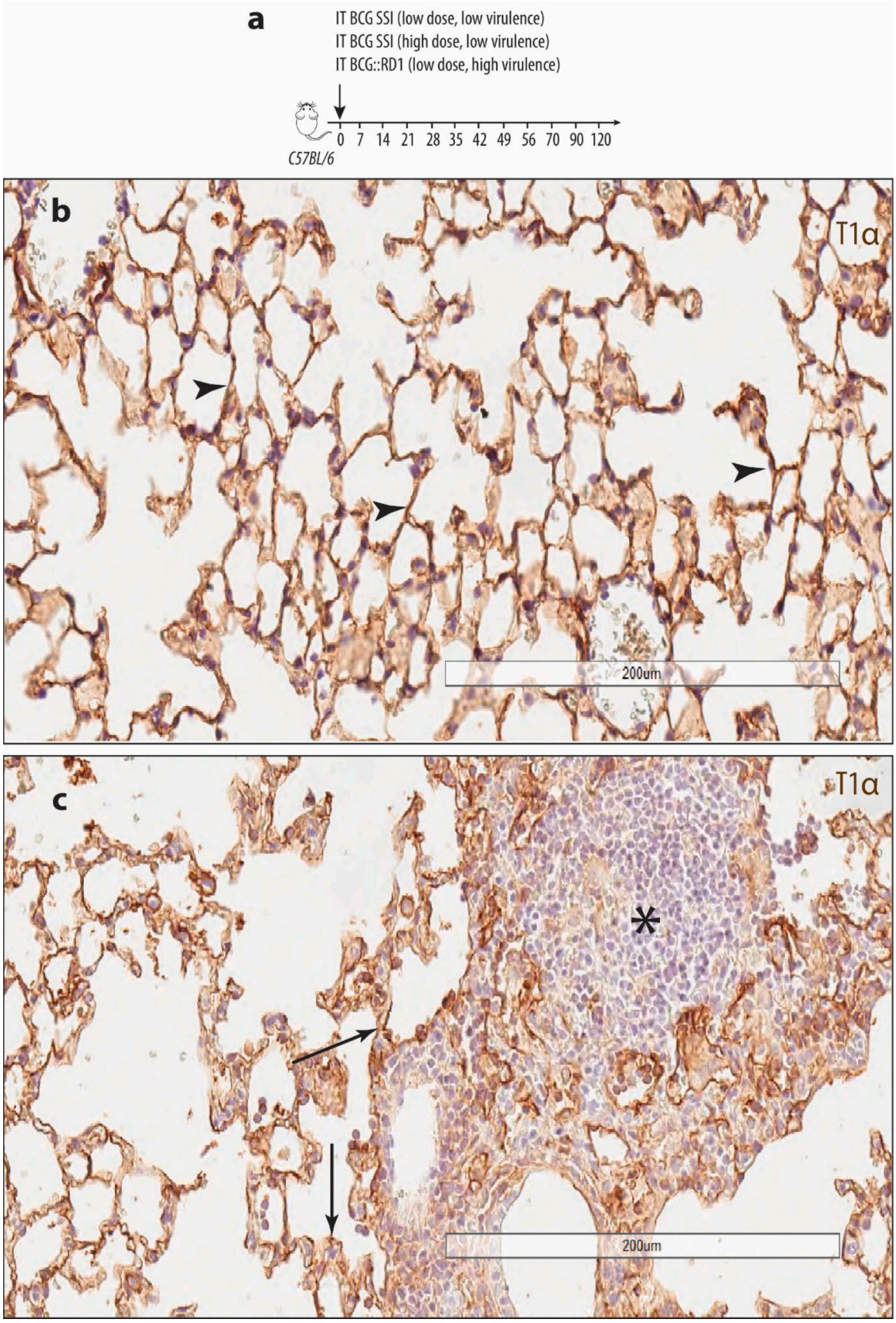

Fig. 1. AEC1 pathology is directly related to IT BCG dose and virulence. a) Experimental design to define AEC pathology across a timeline of 7–120 days past vaccination. **b, c)** Examples of tissue grading of AEC1 using immunohistochemical (IHC) staining for T1α. **b)** Arrowheads indicate normal, thin morphology of AEC1 **c)** asterisk indicates a lesion 21 days past SSI low dose vaccination in which degeneration of AEC1 is evidenced by loss of staining and normal tissue architecture; arrows indicate alveolar wall thickening of AEC1. Results are presented from representative images of 3 mice per time group from two pooled independent experiments (n = 6). **b, c)** Magnification, 20×; Scale bar, 200 μm.

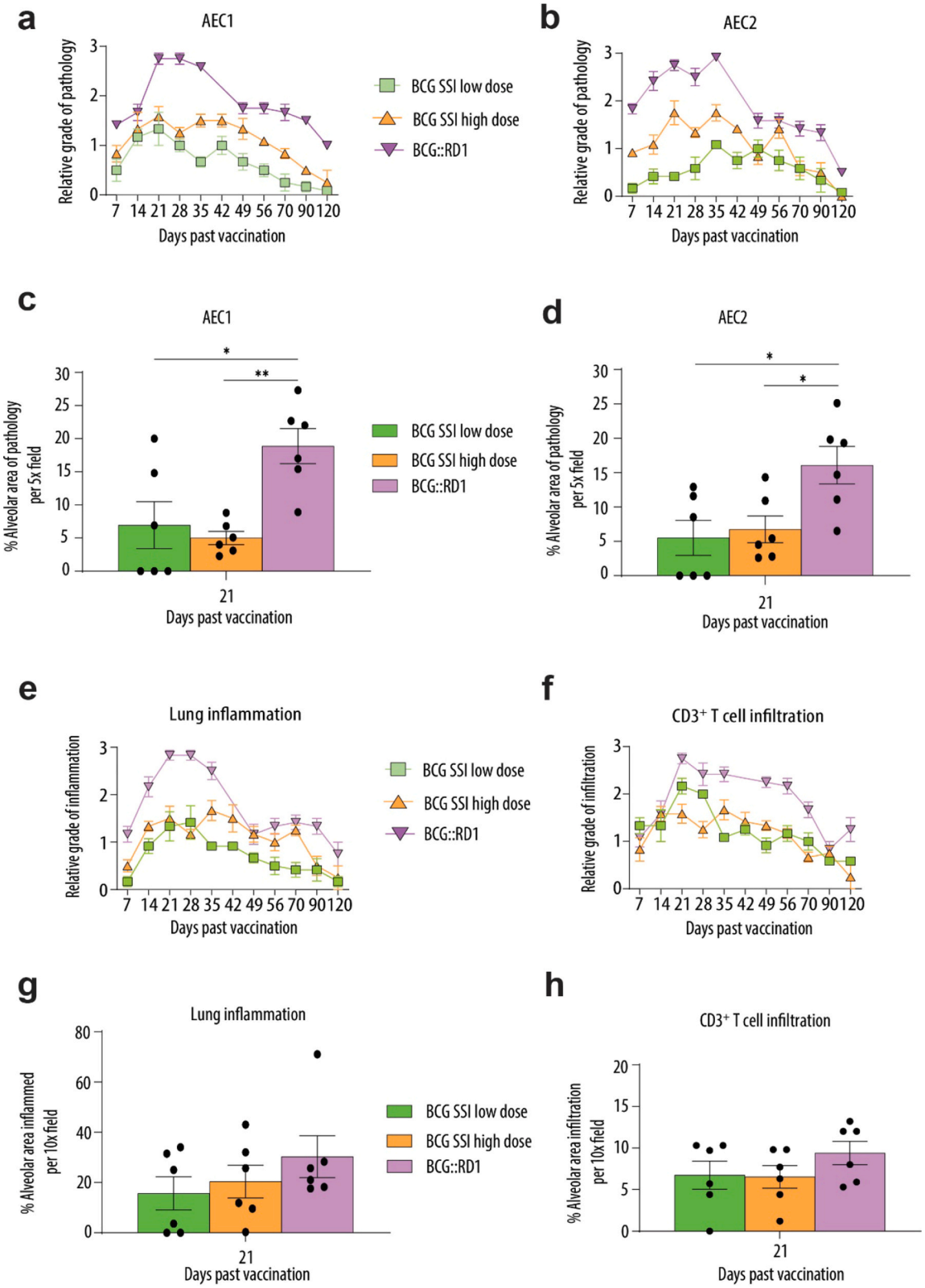

Fig. 2. AEC pathology, lung inflammation, and acquired immune responses are directly related to IT BCG dose, virulence, and delivery. Semi-quantitative enumeration of **a)** AEC1 and **b)** AEC2 pathology from 7-120 days after IT BCG vaccination. **c, d)** Quantification of the alveolar area of AEC pathology at the peak of infection at 21 days past vaccination. Semi-quantitative enumeration of **e)** inflammation and **f)** CD3e infiltration from 7-120 days after IT BCG vaccination. Quantification of the alveolar area of **g)** inflammation and **h)** CD3e infiltration at the peak of infection at 21 days past vaccination. Results are presented from pooled data means ± SEM from 3 mice per time group from two pooled independent experiments (n = 6). $^{*}P < 0.05$; $^{**}P < 0.01$ by One-way ANOVA.

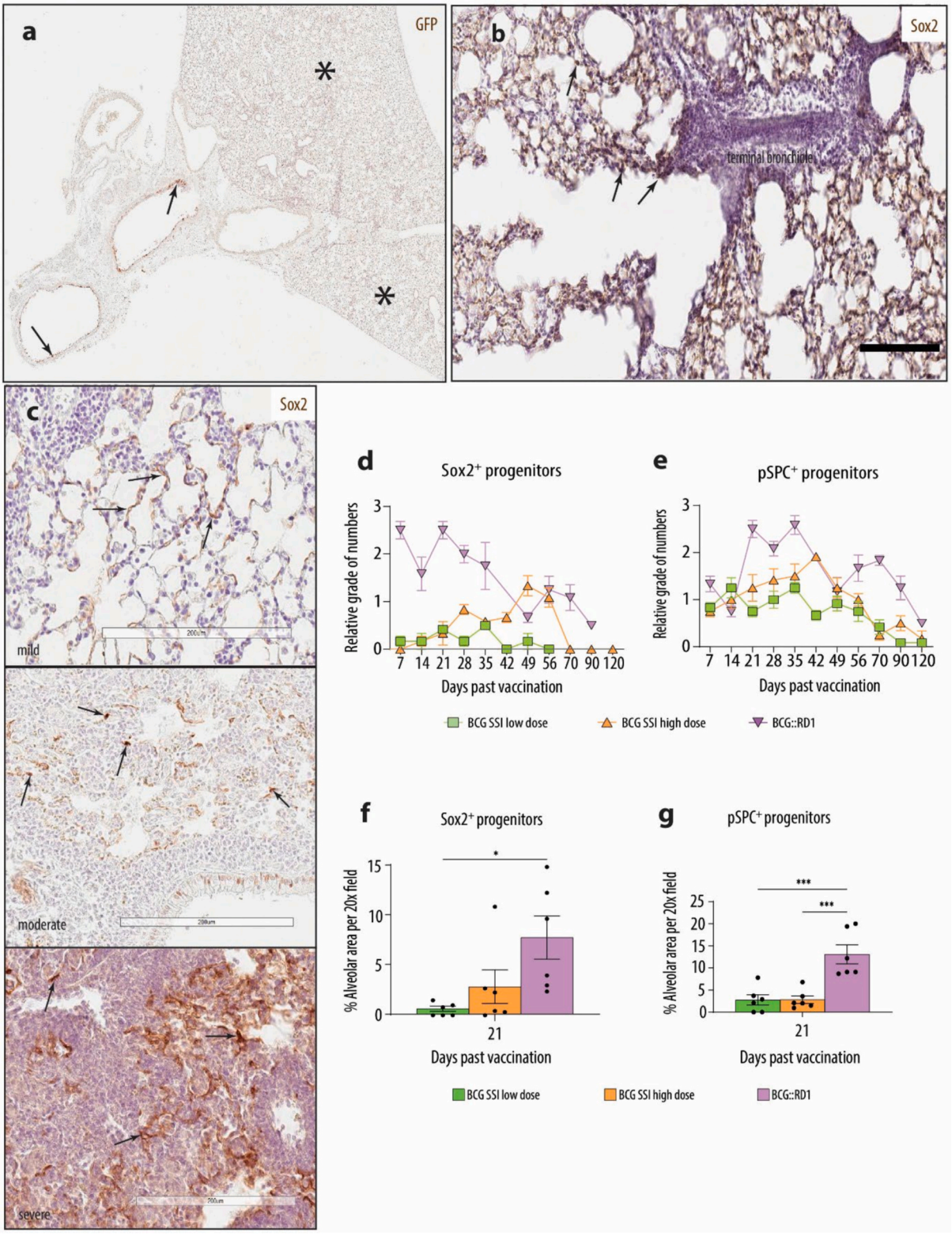

Fig. 3. Sox2^{+} distal airway and pSPC^{+} alveolar progenitors observed after IT BCG vaccination. a) Lung section from *Krt5^{CreERT2}/mTmG* animal 56 days after BCG::RD1 vaccination in which GFP immunoreactivity (indicative of Krt5 expression) was observed in basal cells of the large conducting airways (arrows) but absent in alveolar regions (asterisk) at any timepoint across the 7–120 days after any IT BCG vaccination. **b)** Representative image at 7 days after BCG::RD1 vaccination, where Sox2 expression is seen in cells (arrows) in and adjacent to terminal bronchioles. **c)** Sox2^{+} distal airway progenitors (arrows) were observed throughout all areas of alveolar damage as shown in mild (21 days after BCG::RD1 vaccination), moderate and severe pathology (14 days after BCG::RD1 vaccination). Semi-quantitative enumeration of **d)** Sox2^{+} distal airway and **e)** pSPC^{+} alveolar progenitors from 7-120 days after IT BCG vaccination. **f, g)** Quantification of the alveolar area of Sox2^{+} distal airway and pSPC^{+} alveolar progenitors at the peak of infection at 21 days past vaccination. Results are presented from pooled data means ± SEM from 3 mice per time group from two pooled independent experiments (n = 6). $^{*}P < 0.05$; $^{***}P < 0.001$ by One-way ANOVA. **a)** Magnification, 1.5×; Scale bar 2 mm. **b, c)** Magnification, 10×; Scale bar 200 μm.

dpv and remained severe until 42 dpv (Fig. 2e). T cell infiltration also peaked by 21 dpv and T cells continued to infiltrate with marked numbers until 56 dpv (Fig. 2f). The inflammatory response consisted of haemorrhage secondary to inflammation, marked peribronchiolar and perivascular immune cell infiltrates, and marked numbers of interstitial giant cells and foamy macrophages (Supp. Fig. 5c).

We also observed that at the terminal bronchioles, the BCG SSI high dose vaccine did not induce infiltrating $CD8^+$ T cells (Supp. Fig. 5d). This contrasted with the BCG::RD1 (Supp. Fig. 5e) and low dose BCG SSI (Supp. Fig. 5f) vaccinations. We reasoned that higher numbers of bacilli caused them to aggregate into flocs making the particulate matter of the vaccine larger and therefore the BCG SSI high dose vaccine was not delivered into the distal airways and alveoli[43]; indeed, lungs sectioned up to proximal airways showed infiltration of $CD8^+$ T cells in peribronchiolar regions (Supp. Fig. 5g). When we had established that the peak of tissue damage was 21 dpv following all vaccinations, we quantified these two immune responses (Fig. 2g, h) to demonstrate that dose, virulence, and depth of delivery of mucosal BCG vaccination had direct effects on inflammation and acquired CD3 T cell responses.

Only $Sox2^+$ distal airway and $pSPC^+$ alveolar epithelial progenitors respond to AEC losses associated with mucosal BCG vaccination

We next undertook an original characterization of lung epithelial progenitor cell responses to tissue damage associated with mucosal BCG vaccinations. Lung sections were probed using antibodies against Krt5 for DASC, Sox2 for distal airway epithelial progenitors and pSPC for alveolar epithelial progenitors across the timeline. Although Krt5 was expressed in basal cells of the large airways, $Krt5^+$ cells were not observed in alveolar tissue at any time after vaccination (Supp. Fig. 6a). We confirmed this using $Krt5^{CreERT2}/mTmG$ reporter mice to tag $Krt5^+$ DASC progeny with green fluorescent protein (GFP).[44] Again, we observed GFP in the large airway basal cells but never in alveolar tissue after any vaccination (Fig. 3a).

In contrast, by 7 dpv after BCG::RD1 vaccination, cells with$Sox2^+$ expression were observed in terminal bronchioles and in contiguous alveolar epithelium (Fig. 3b); of note, $Sox2^+$ cells were observed throughout all areas of alveolar damage across all the vaccinations (Fig. 3c). Therefore, across the timeline of vaccinations, relative enumeration of $pSPC^+$ alveolar epithelial (Supp. Fig. 6b) and $Sox2^+$ distal airway progenitors (Supp. Fig. 6c) was undertaken with progenitor proliferation (hyperplasia) graded as none (Grade 0), minimal

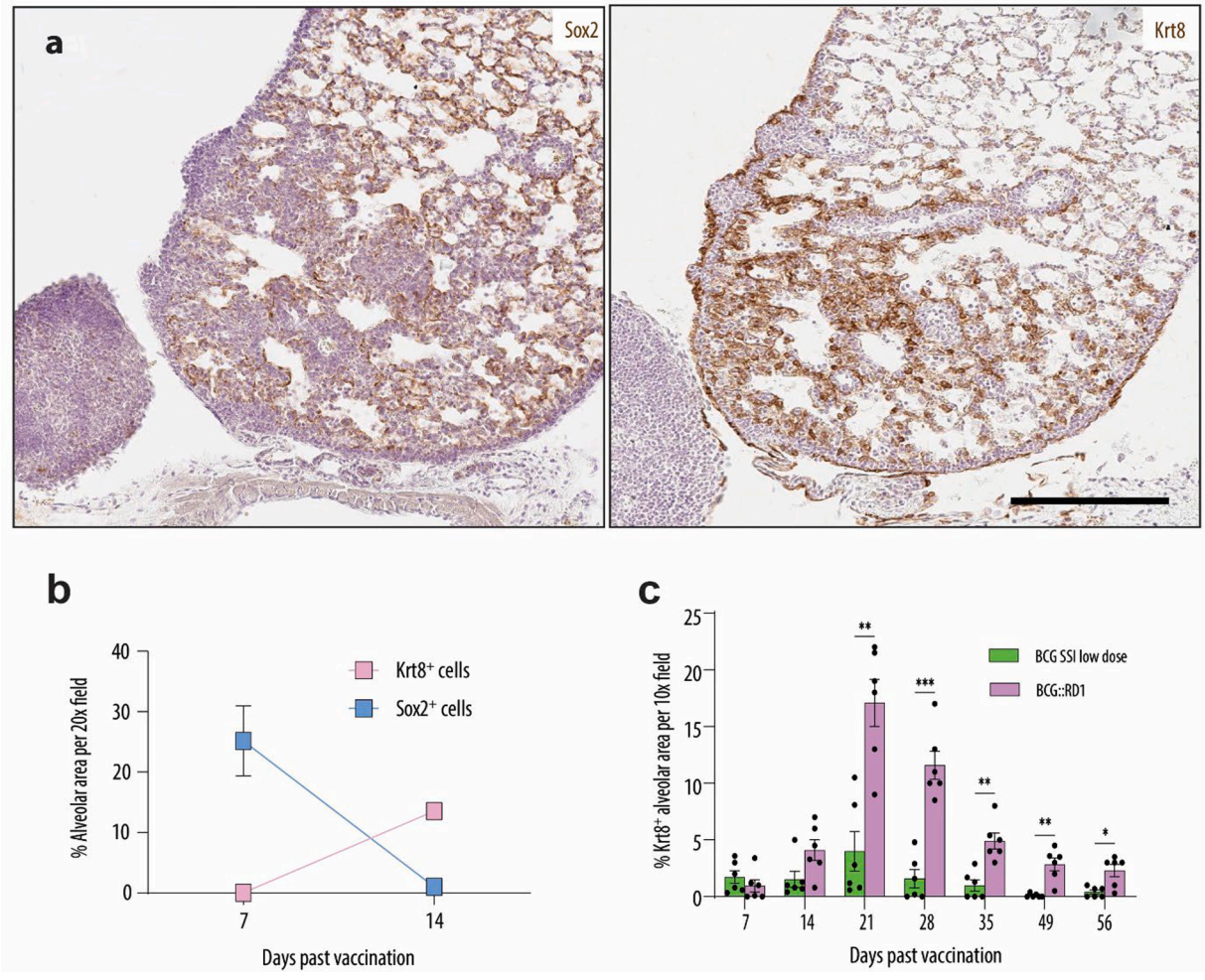

Fig. 4. Activation of $Sox2^+$ distal airway and $Krt8^+$ transitional progenitors is dependent upon dose and virulence of IT BCG vaccination. a) Krt8 IHC staining revealed that the transitional progenitor state was observed within tissue areas of Sox2 expression, in an 'inverse' relationship seen here at 14 days after vaccination with BCG::RD1. Results are presented from representative images from 3 mice per group from two pooled independent experiments (n = 6). **b)** Quantification of the alveolar area $Sox2^+$ and $Krt8^+$ progenitor cell infiltration at 7 and 14 days after BCG::RD1 vaccination to verify their inverse temporal relationship. **c)** Quantification of $Krt8^+$ TP numbers at the peak of infection at day 21 after vaccination with BCG::RD1. Results are presented from representative images and data means ± SEM from 3 mice per group from two pooled independent experiments (n = 6). $^*P < 0.05$; $^{**}P < 0.01$; $^{***}P < 0.001$ by unpaired Student's *t* test. **a)** Magnification, 10×; Scale bar 200 μm.

(Grade 1), moderate (Grade 2) or marked (Grade 3). While this relative enumeration of progenitors was underway, a Krt8$^+$ transitional progenitor (TP) cell state that precedes differentiation of both Sox2$^+$ airway and pSPC$^+$ progenitors into AEC1 was described,[32,35,36] thus we included investigation of Krt8$^+$ TP using our IT BCG vaccinations as we reasoned that these are the epithelial progenitors that interact with lung CD8$^+$ T cells.

Results demonstrated that following the BCG::RD1 vaccination marked Sox2$^+$ airway progenitors were observed early (Fig. 3d) but waned after day 21; conversely, marked pSPC$^+$ alveolar progenitors were observed after day 21 (Fig. 3e). Following BCG SSI high dose vaccination, Sox2$^+$ airway progenitors peaked at 49 dpv (Fig. 3d) and were confined to proximal peribronchiolar regions. After BCG SSI low dose vaccination, Sox2$^+$ cell numbers were minimal (Fig. 3e) while pSPC$^+$ progenitors (Supp. Fig. 6b) appeared largely as doublets with 'foci' of cells across neighbouring alveoli described by Desai *et al.*.[28] We quantified numbers of progenitor populations at the peak of infection (21 dpv) and observed numbers of Sox2$^+$ distal airway progenitors and pSPC$^+$ alveolar progenitors were significantly higher after BCG::RD1 vaccination compared to the BCG SSI vaccinations (Fig. 3f, g).

Using serial sections, we observed an inverse staining pattern in which alveolar areas void of Sox2 staining had Krt8 staining and vice versa (Fig. 4a). This supported the notion that Sox2$^+$ distal airway cells were transitioning into Krt8$^+$ progenitors. Thus, we quantified Sox2$^+$ and Krt8$^+$ cells at 7 and 14 dpv to verify this inverse relationship (Fig. 4b). By 14 dpv, the BCG SSI low dose had punctate areas of Krt8$^+$ TP (Supp. Fig. 7a), while the BCG::RD1 vaccination had broad diffusion of Krt8$^+$ TP throughout lungs (Supp. Fig. 7a). At 21 dpv after BCG SSI low dose, Krt8$^+$ cells acquired a squamous morphology and were likely transitioning into AEC1 (Supp. Fig. 7b); conversely, after BCG::RD1 vaccination, Krt8$^+$ cells remained round (Supp. Fig. 7b) and did not become squamous until after 28 dpv (data not shown). Quantification of Krt8$^+$ TP for both vaccinations showed a peak of Krt8$^+$ TP at 21 dpv where BCG::RD1 vaccinated lungs had an average alveolar area of ~ 20% occupied by Krt8$^+$ cells, while those of the SSI low dose had an area of ~ 5% (Fig. 4c).

In summary, responses of alveolar epithelial progenitors, distal airway epithelial progenitors, and DASC to alveolar epithelial cell loss associated with mycobacterial lung injury were unknown at the start of this research. Knowing the effects that RD1 virulence factors have on AEC, we at first presumed that vaccination with BCG::RD1 may cause a similar lung injury healing sequalae as reported after virulent influenza (PR8) infection in mice.[19,21,22,33,45] Our findings, instead, describe sequalae in which Sox2$^+$ distal airway progenitors migrated into alveolar tissues to orchestrate restitution in areas where facultative alveolar epithelial progenitors were lost due to the virulence factors of RD1. Conversely, mucosal lung exposure to doses of non-virulent BCG resulted in efficient regeneration of lost epithelium by local alveolar epithelial progenitors. Both distal airway and alveolar progenitor cell types likely transitioned through the Krt8$^+$ TP state into AEC1, evidenced by near complete tissue restitution at 120 dpv.

Lung CD8$^+$ T_{RM} induction depends on BCG virulence and dose

Paucity of literature about CD8$^+$ T_{RM} in the lungs following mycobacterial (and other intracellular bacterial) infection, motivated us to also unravel the kinetics of the establishment of CD8$^+$ T_{RM} and their persistence in lungs after different types of mucosal BCG vaccination. Mice were given IT BCG vaccination as described; whole lungs of experimental animals were harvested and processed into single-cell suspensions before flow cytometry (Supp. Fig. 8) and quantification using recognised lung CD8$^+$ T_{RM} markers. Of note, our previous studies have shown that only mucosal IT BCG vaccination, but not SC BCG vaccination generates lung CD8$^+$ T_{RM} and that those cells are mycobacteria-specific.[11]

BCG::RD1 vaccination led to robust expansion of CD8$^+$ T_{RM} from days 14–35 dpv, with a peak at day 28; numbers contracted at day 35 yet remained high until 120 days (Fig. 5a, b). Of the three subsets of T_{RM}, CD103$^+$CD69$^+$CD49a$^+$ T_{RM} cells that patrol airway/ interstitial borders[46] were the highest proportion at 45% of total CD8$^+$ T cells at their peak at 28 dpv (Fig. 5a, b). Interstitial CD103$^-$CD69$^+$CD49a$^+$ T_{RM}[46,47] were also abundant (Fig. 5a, b) while the short-lived CD103$^+$CD69$^+$CD49a$^-$ T_{RM} that solely patrol the airways[46,48] were less (Fig. 5a, b). CD103$^-$CD69$^+$CD49a$^-$ T_{RM} precursor cells[47] were continually present in the lung from day 14–120 (Fig. 5a, b).

After vaccination with a high dose of BCG SSI, CD8$^+$ T cells in the lung were half the numbers seen following BCG::RD1 vaccination (Fig. 5a, b). Of those, 25 % were CD103$^+$CD69$^+$CD49a$^+$ T_{RM} at day 21 dpv (Fig. 5a, b) while CD103$^+$CD69$^+$CD49a$^-$ airway effector T_{RM} were higher than those seen after BCG::RD1 vaccination (Fig. 5a, b). BCG SSI low dose vaccination induced only about a third of CD8$^+$ T cells in the lung compared to BCG::RD1 vaccination (Fig. 5a, b). Of those, 10% were CD103$^+$CD69$^+$CD49a$^+$ T_{RM} at day 21 dpv (Fig. 5a, b) and waned each week. In line with our previous results,[11] there were significantly higher numbers of all CD8$^+$ T_{RM} subsets following BCG::RD1 vaccination compared to BCG SSI low dose vaccination, particularly from 14 to 28 dpv (Fig. 5c-f).

Taken together, our results show that lung CD8$^+$ T_{RM} induction is virulence- and dose-related and that CD8$^+$ T_{RM} wane in the lungs by 120 days after mucosal BCG vaccination.

Lung-draining mediastinal lymph node harbor cells with CD8$^+$ T_{RM} phenotypes following mucosal BCG vaccination

It has been consistently demonstrated that lung CD8$^+$ T_{RM} wane over a short time,[10,49–51] despite continual circulation of antigen-specific T cells in blood.[20] As lung CD8$^+$ T_{RM} are known to egress to the lung-draining mediastinal lymph node (mLN), we next investigated whether mLN contain CD8$^+$ T_{RM} following mucosal BCG vaccination, as this was unknown. Mice were given IT vaccination, the right superior mLN was extracted from all experimental animals across 7–120 dpv and processed into single-cell suspensions before quantification of CD8$^+$ T_{RM} using flow cytometry.

We discovered all phenotypes of CD8$^+$ T_{RM} in the mLN. CD103$^+$CD69$^+$CD49a$^+$ were conceivably swept into lymphatics due to tissue damage that physically dislodged them,[52] a notion supported by the significantly higher numbers of this subset at 14 dpv (a time of severe tissue damage) following BCG::RD1 vaccination as compared to BCG SSI low dose vaccination (Fig. 6a). Both interstitial CD103$^-$CD69$^+$CD49a$^+$ T_{RM}, in which lack of CD103 maturation is said to contribute to their egression to the mLN[52] and airway CD103$^+$CD69$^+$CD49a$^-$ T_{RM} were enumerated at significantly higher numbers 42 dpv after BCG::RD1 compared to BCG SSI low dose vaccination (Fig. 6b, c). Numbers of CD103$^-$CD69$^+$CD49a$^-$ early activated precursor T_{RM} were also significantly higher at 14 and 21 dpv following BCG::RD1 compared to BCG SSI low dose vaccination (Fig. 6d). We report for the first time that following mucosal BCG vaccination, mLN harbor cells with CD8$^+$ T_{RM} phenotypes for at least 4 months. Egression of CD8$^+$ T_{RM} from the lung to the mLN is a recently described phenomenon and further experiments will be required to authenticate the mechanisms associated with possible ex-lung T_{RM} egression after mucosal BCG immunisation.

Distal airway progenitor cells provide paracrine cues for the induction and persistence of CD8$^+$ lung T_{RM} cells following mucosal BCG vaccination

The sum of our analyses inferred that a mechanism of induction and maintenance of lung CD8$^+$ T_{RM} may be linked to the tissue milieu associated with alveolar damage. Therefore, we investigated putative relationships between lung epithelial progenitor cells and CD8$^+$ T_{RM} following mucosal BCG vaccination as we hypothesized that distal airway progenitor cells provide a paracrine induction cue for lung CD8$^+$

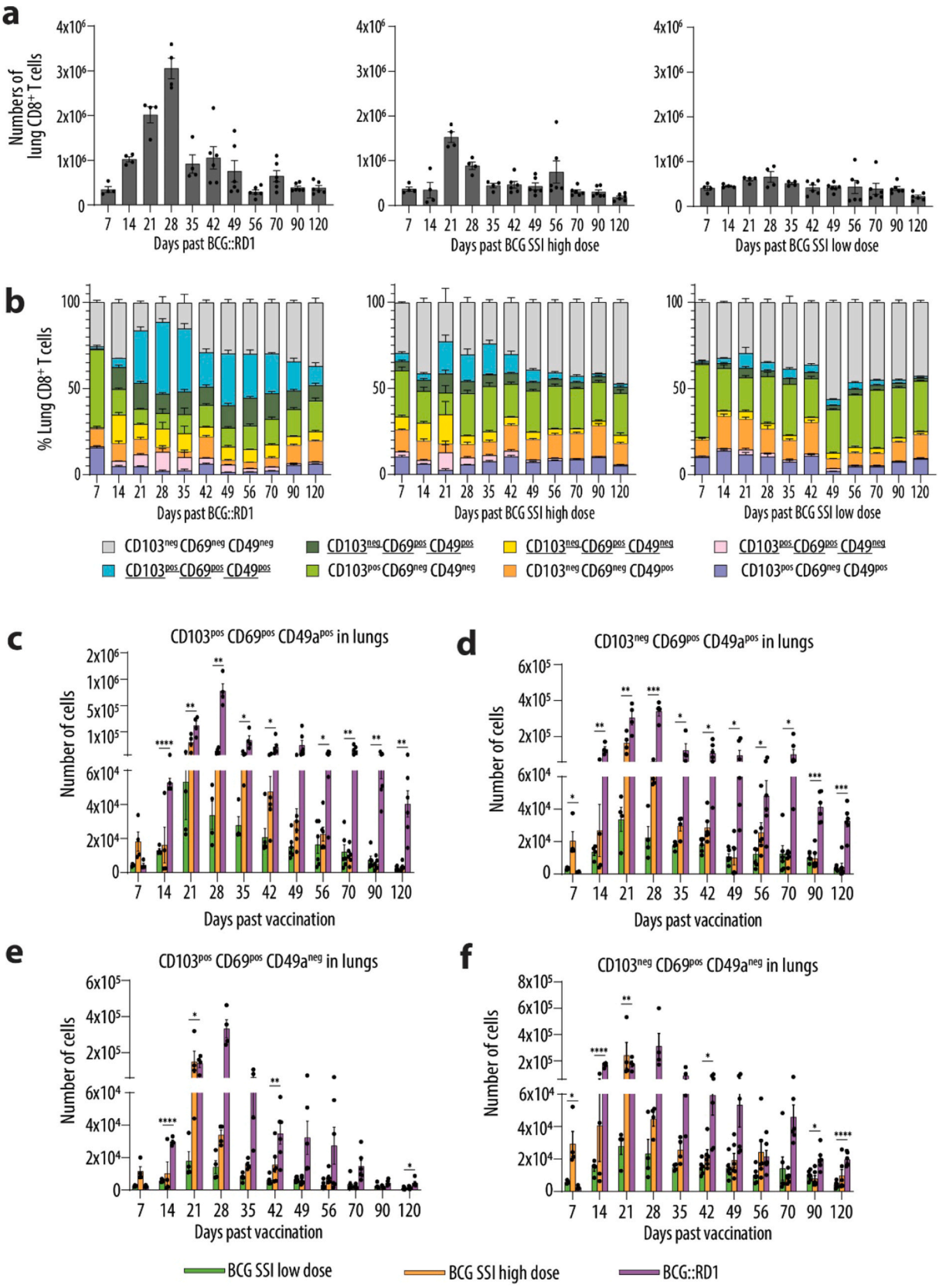

Fig. 5. CD8$^+$ T cell numbers and percentages of lung CD103, CD69 and CD49a T_{RM} subsets across models of mucosal BCG vaccination. Flow cytometry analysis across the timeline from 7-120 days after vaccination for **a)** numbers of CD8α$^+$ T cells, **b)** the percentages of CD8$^+$ T_{RM} subsets (underlined) and **c-f)** numbers of CD8$^+$ T_{RM} subsets in the lungs of vaccinated mice. Pooled data from two independent experiments where n = 4–10 for each timepoint. *$P < 0.05$; **$P < 0.01$; ***$P < 0.001$; ****$P < 0.0001$ by unpaired Student's *t* test between BCG::RD1 and BCG SSI high dose or BCG::RD1 and BCG SSI low dose. Comparison of BCG SSI vaccinations had no significance by unpaired Student's *t* test.

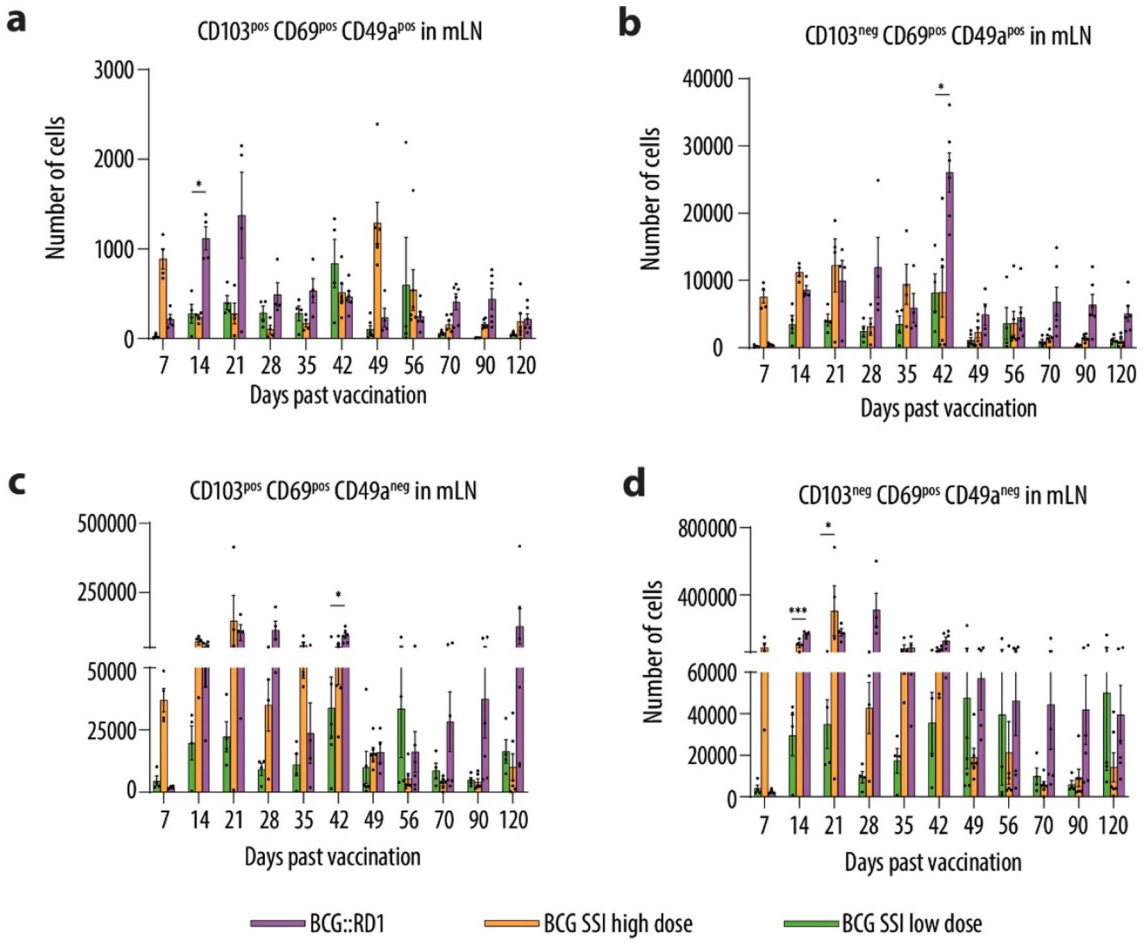

Fig. 6. CD8$^+$ T_{RM} counts in mLN after mucosal BCG vaccinations. a-d) Flow cytometry quantification of CD8$^+$ T_{RM} subsets in mLN of vaccinated mice from day 7–120 after vaccination. Pooled data of mLN CD8$^+$ T_{RM} from two independent experiments where n = 4–10 for each timepoint. *$P < 0.05$; ***$P < 0.001$ by unpaired Student's *t* test.

T_{RM}. As described in influenza mouse models, CD8$^+$ T_{RM} form in areas of severe alveolar destruction, precisely the areas into which airway progenitor cells home[20,21,27,34,53]; so, we first investigated spatial and temporal relationships of Krt8$^+$ TP and CD8$^+$ T_{RM} using imaging analyses across all vaccination models. We visualized evident structural and temporal localization, particularly in areas of severe tissue damage (Fig. 7a). Given that BCG::RD1 was associated with the most severe tissue damage, we used vaccination with BCG::RD1 to dissect mechanistic relationships between distal airway epithelial progenitor cells and immune memory.

TGF-β upregulates the CD8$^+$ T_{RM} transcriptome[54,55] and a key activator of latent TGF-β in lungs is integrin αVβ6.[56] As stated previously, repair and regeneration of the lung after significant injury involves expansion and migration of both residual alveoli and airway-derived stem/progenitor cells. In the mouse, after bleomycin injury, approximately half of the mature AEC2s present in the recovered lungs derive from distal airways or bronchioalveolar junctions.[31,57] Distal airway cells, once mobilised, migrate and cover large areas of denuded or heavily damaged alveolar epithelium and then restore normal alveolar epithelium.[31] It is these distal airway and Krt8$^+$ transitional progenitors that express αVβ6[32,46,58]; after bleomycin injury, Auyeung *et. al.* found that Krt8$^+$ TP accounted for the majority of cells expressing integrin αVβ6.[58] Moreover, Strunz *et. al.* showed that αVβ6 is only expressed in Krt8$^+$ TP just after the peak of Krt8 expression and before terminal differentiation into AEC1.[32] Knowing that lung epithelial progenitors express αVβ6[20,32,58,59] and that latent TGF-β is stored in the lung ECM in high concentrations,[56,60] we hypothesized that as airway epithelial progenitor cells home into hypoxic alveolar tissue, they activate interstitial latent TGF-β which subsequently may bind TGF-β receptors on adjacent CD8$^+$ T cells and induce the CD8$^+$ T_{RM} transcriptome (Fig. 7b). To first test this hypothesis, we quantified lineage traced Sox2$^+$ distal airway progenitors at 120 dpv in regenerated alveolar tissue, using *Sox2^{CreERT2}:B6.Cg-Gt(ROSA)26Sor$^{tm14(CAG-tdTomato)Hze}$/J* (aka *Sox2/Ai14*) reporter mice in which progeny of Sox2$^+$ distal airway progenitors were indelibly tagged with red fluorescent protein (RFP)(Fig. 7c). To ensure there was no tamoxifen persistence, tamoxifen was administered 28 days prior to IT BCG vaccination.

We observed that numbers of lineage traced AEC1 and AEC2 following BCG::RD1 vaccination were 6 and 8-fold higher, respectively, than those observed after BCG SSI low dose (Fig. 7d); therefore, the number of lineage traced Sox2$^+$ distal airway epithelial progenitors in regenerated alveolar tissue was significantly higher following mucosal BCG::RD1 vaccination. We next visualized and quantified extracellular interstitial alveolar tissue active TGF-β from 7 to 21 dpv when Sox2$^+$ distal airway epithelial progenitors were at peak numbers in the tissue. Results showed that BCG::RD1 vaccinated animals had peribronchiolar interstitial active TGF-β expression as early as 7 dpv and by 14 dpv alveolar interstitial expression was evident (Fig. 7f). By 21 dpv, alveolar interstitial expression was global, and areas of severe damage had significantly higher expression (Fig. 7g).

Animals vaccinated with BCG SSI high dose had sparse peribronchiolar expression of active TGF-β from 14 to 21 dpv with early, extracellular airway expression (Fig. 7h). In animals vaccinated with the low dose of BCG SSI, only few alveolar macrophages had cytoplasmic

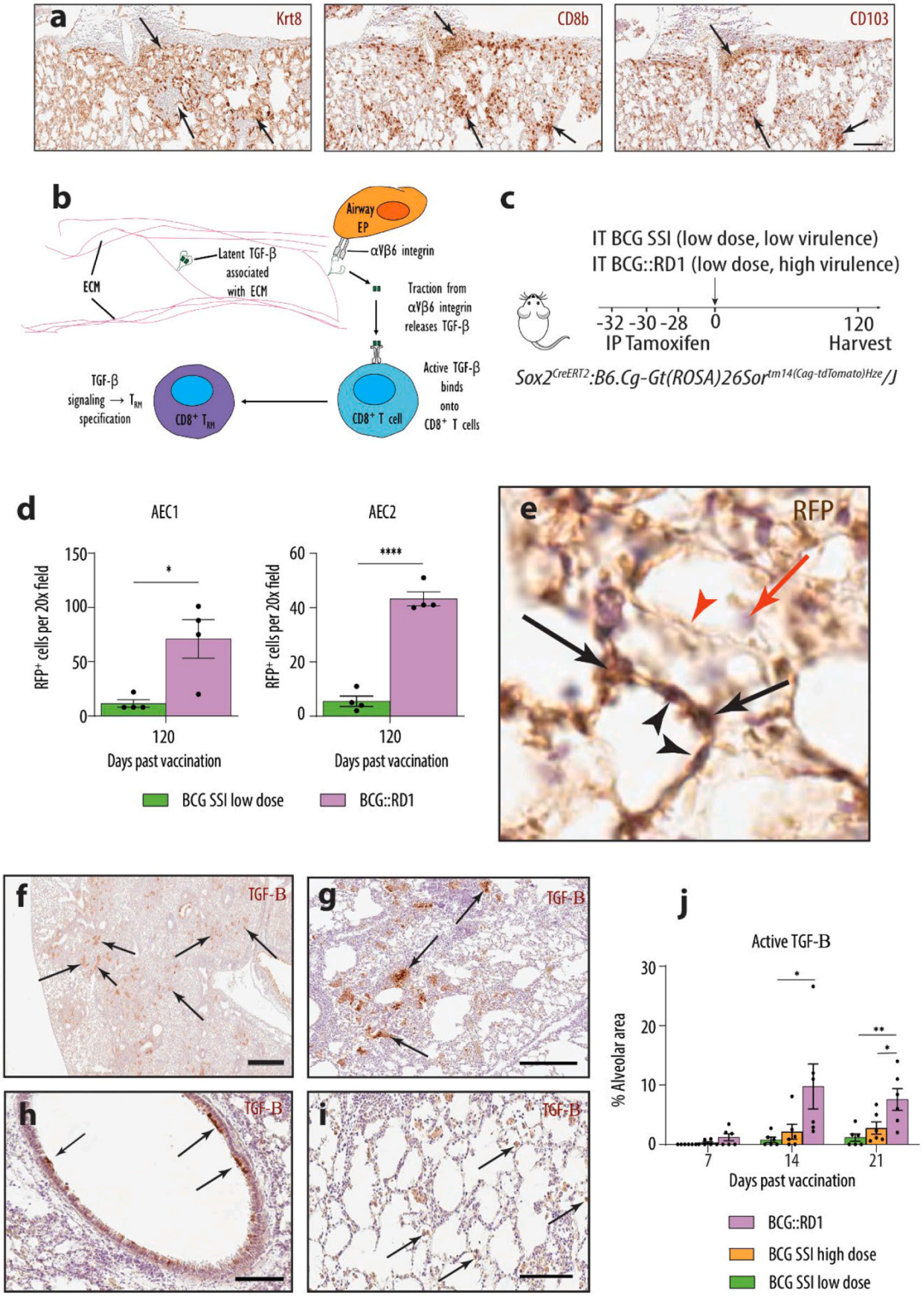

Fig. 7. Distal airway epithelial progenitors have a role in the release of alveolar tissue active TGF-β. a) Demonstrative serial micrographs show spatial and temporal localization of Krt8^{+} TP with CD8b^{+}CD103^{+} T cells in areas of severe alveolar damage at day 21 after vaccination with BCG::RD1. **b)** Model of interaction between airway epithelial progenitors and adjacent CD8^{+} T cells. **c)** Experimental design for lineage tracing of *Sox2/Ai14* progeny and **d)** their quantification at 120 days after vaccination. **e)** Sox2 lineage traced AEC1 (black arrowheads) and AEC2 (black arrows) compared to RFP negative AEC1 (red arrowhead) and AEC2 (red arrow) at 120 days after vaccination. Alveolar interstitial tissue active TGF-β following IT vaccination with BCG::RD1 observed in **f)** distal alveolar interstitium (arrows) at 14 days and **g)** areas of severe damage (arrows) at 21 days after vaccination**. h)** Bronchiolar airway expression (arrows) of active TGF-β at 14 days after IT SSI high dose vaccination. **i)** Only the cytoplasm of alveolar macrophages (arrows) exhibited active TGF-β at 21 days after IT SSI low dose vaccination; there was no alveolar interstitial active TGF-β expression seen in any animals at any timepoint examined. **j)** Quantification of extracellular alveolar interstitial active TGF-β at 21 days following IT BCG vaccinations. Pooled data from two experiments where n = 6 for each timepoint. $^{*}P < 0.05$; $^{**}P < 0.01$ by One-way ANOVA**. a)** Magnification, 20×; Scale bar 100 μm. **f)** Magnification, 4×; Scale bar 600 μm. **g)** Magnification, 11.6×; Scale bar 200 μm. **h)** Magnification, 20×; Scale bar 100 μm. **i)** Magnification 20×; Scale bar 100 μm. (For interpretation of the references to colour in this figure legend, the reader is referred to the web version of this article.)

expression of active TGF-β (Fig. 7i); there was no alveolar interstitial expression of active TGF-β observed. Quantification showed that after BCG::RD1 vaccination, alveolar tissue active TGF-β was significantly more concentrated at the time when Sox2$^+$ distal airway epithelial progenitors populate severely damaged epithelium (Fig. 7j).

Worth stating, we also sought to quantify lineage traced AEP at 120 dpv in regenerated alveolar tissue using *Axin2$^{CreERT2:TdT}$/EYFP* reporter mice to tag AEP progeny with yellow fluorescent protein (Supp. Fig. 9a). At tissue harvest at 56 or 120 dpv, however, animals had an atypical response to the BCG::RD1 across four experiments, despite no known underlying genetic abnormality. Lesions of these lungs contained Krt8$^+$ TP, AEP and interestingly, Krt5$^+$ DASC progeny as well as profuse alveolar interstitial active TGF-β (Supp. Fig. 9b). The observed Krt5$^+$ cells in dysplastic lung lesions were primarily interstitial and not adjacent to bronchioles (as described in the murine PR8 influenza model). We did not observe the development of dysplasia following any of the other three IT vaccinations with BCG; rather, in the C57BL/6, *Sox2-^{CreERT2}/Ai14*, and *Krt5^{CreERT2}* mice, the epithelial progenitors successfully transitioned from the Sox2$^+$ and pSPC$^+$ phenotypes through the Krt8$^+$ TP state and differentiated into AEC1 and AEC2 (evidenced by overall lung restitution).

Itgβ6 knock out mice develop significantly fewer CD8$^+$ T_{RM} following mucosal vaccination with BCG::RD1

To more directly test our hypothesis that distal airway epithelial progenitor cell-mediated release of TGF-β has a role in the induction of CD8$^+$ T_{RM}, we used knock-out (KO) mice that lacked a functional αVβ6 integrin.[61,62] *Integrin beta-6 (ItgB6)* KO mice were vaccinated with BCG::RD1 and tissues harvested across 7–35 dpv (Fig. 8a). We confirmed levels of injury in the *ItgB6* KO mice were comparable to C57BL/6 wild type mice using histology (Supp. Fig. 9c, d) and quantification of Krt8$^+$ TP numbers (Fig. 8b). We then compared alveolar extracellular interstitial active TGF-β, as *ItgB6* KO airway progenitor cells would be unable to activate latent TGF-β. At 21 dpv (the peak of Krt8$^+$ progenitor numbers), we observed that C57BL/6 mice had an area of ~ 8% interstitial active TGF-β, compared to the *ItgB6 KO* animals which had significantly less at ~ 1% (Fig. 8d, e).

We next quantified CD8$^+$ T_{RM} subsets and their proportions in the lungs of the *ItgB6* KO animals after BCG::RD1 vaccination across 5 weeks and found that while C57BL/6 mice had a 25% increase in all CD8$^+$ T_{RM} between 14–21 dpv (Supp. Fig. 9e), the *ItgB6* KO animals only had an increase of 5% (Supp. Fig. 2f). This smaller increase was even though the KO mice had more lung CD8$^+$ T cells at 14 dpv and the same number as WT at 21 dpv (Supp. Fig. 9 g). We also observed that CD103-expressing CD8$^+$ T_{RM} subsets were specifically significantly decreased in *ItgB6* KO animals after BCG::RD1 vaccination compared to WT animals (Fig. 8f), consistent with the role of TGF-β in upregulation of CD103 expression in CD8$^+$ T cells.[54,63]

To investigate the relationship between αVβ6$^+$ distal airway epithelial progenitor-mediated release of TGF-β, and subsequent induction of CD8$^+$ T_{RM} for immune protection against TB, we compared C57BL/6 wildtype and *ItgB6* KO mice that were challenged aerogenically with *Mtb* sixty days after mucosal BCG::RD1 vaccination. The bacterial loads in lungs and spleen as well as *Mtb*-mediated damage to lung tissue were determined at 45 days after *Mtb* infection (Fig. 8g). Histological analyses revealed that the lungs of BCG::RD1 vaccinated *ItgB6* KO animals showed severe pathology comparable with all unvaccinated animals where ~ 40% of lung was affected by *Mtb* infection (Fig. 8h, i). Although we had hypothesised that *ItgB6* KO would have significantly increased CFU compared to wild type mice (linked to decreased numbers of CD8$^+$ T_{RM}), interestingly, in *ItgB6* KO BCG::RD1 vaccinated mice, CFU counts in the spleen were significantly lower than unvaccinated animals and unremarkable compared to vaccinated C57BL/6 wild type mice. Additionally, *ItgB6* KO BCG::RD1 vaccinated lung CFU counts were also significantly lower than not only the unvaccinated animals, but also the BCG::RD1 vaccinated wild type mice (Fig. 8j). An explanation for the disparity between lung pathology and CFU counts in the BCG::RD1 vaccinated *ItgB6* KO mice may be linked to the lack of interstitial active TGF-β (necessary for fate specification and differentiation of T_{RM} cells) which thus drove early memory precursor effector cells down the differentiation pathway into circulatory effector memory T cells (T_{EM}).[20] Upon secondary infection, CD8$^+$ T_{EM} exhibit immediate potent cytotoxic effector functions[64] and indeed, the percentages of CD8$^+$ T_{EM} in BCG::RD1 vaccinated *ItgB6* KO mice were 25–30% of total lung CD8$^+$ T cells from 21 to 35 dpv, compared to C57BL/6 BCG::RD1 vaccinated mice which had 12–15% over the same time period (Supp. Fig. 9e, f).

It was not wholly unexpected that the *ItgB6* KO mice had increased protection against TB challenge following BCG::RD1vaccination as they have been shown to be protected from diverse respiratory infections.[65,66] *ItgB6* KO lungs harbor constitutively activated lung CD11b$^+$ alveolar macrophages and elevated type I IFN signaling activity, linked to the loss of β6-activated TGF-β; even in the absence of infection, *Itgβ6* KO animals have a distinct anti-microbial lung microenvironment.[65] Additionally, a consensus in the field is that vaccine-mediated reduction of *Mtb* burden depends on multiple complex redundant and overlapping immune responses with a strong CD4$^+$ T cell component.[67–71] Our results do indicate, however, that CD8$^+$CD103$^+$ T_{RM} directly contribute to prevention of *Mtb*-induced lung pathology.

In conclusion, following mucosal BCG vaccination, Krt8$^+$ TP were structurally and temporally localised with CD8$^+$CD103$^+$ T_{RM} in alveolar tissue, active TGF-β was widespread throughout the alveolar interstitium following BCG::RD1 vaccination in which significantly higher numbers of lineage-traced distal airway progenitors were shown. When αVβ6 integrin was knocked out, and importantly, active TGF-β was absent, CD8$^+$CD103$^+$ T_{RM} numbers significantly decreased. Taken together, these findings support a model in which distal airway epithelial progenitor-mediated release of TGF-β has a role in the induction and persistence of protective lung CD8$^+$ T_{RM} cells following mucosal BCG vaccination.

Discussion

TB is a global health burden and one of the major causes of human death; thus, a new vaccine that induces lung-resident mucosal immunity is urgently needed. This work elucidated a mechanism by which local delivery of BCG into the airways induces resident mucosal immune memory in the lungs which holds several important implications for the development of a more effective TB vaccine.

Firstly, mucosal BCG is known to induce better systemic and mucosal immune responses compared to subcutaneous BCG in animals.[8,10,72,73] Recent dose-escalation studies with aerosolised BCG in humans established a safe and well tolerated dose and reported no significant differences in the frequency of adverse events between groups that received either inhalation or injection of BCG.[74] The study suggests the possibility of BCG vaccine administration by inhalation to humans—a strategy known to induce robust lung immunity in animals.

Another key strategy to improve the efficacy of the TB vaccine is BCG modifications that generate a more persistent CD8$^+$ T cell memory. The BCG::RD1 construct used in our studies is known to protect animals from TB challenge following mucosal administration; here, we showed for the first time that mucosally administered RD1 virulence factors had a direct influence on the severity and extended time of AEC losses, inflammation and subsequent CD8$^+$ T cell responses and ultimately, tissue regeneration. The virulence factors of RD1 were further linked to the effects of lung regeneration by epithelial progenitor cells and, by extension, the establishment of tissue resident memory CD8$^+$ T cells. Our findings drive forward novel conceptual insights into how lung regeneration and tissue immunity are linked at the cellular/molecular level.

Although there remains optimism in the field that numbers of vaccine induced CD8$^+$ T_{RM} against *Mtb* could be made to persist in the

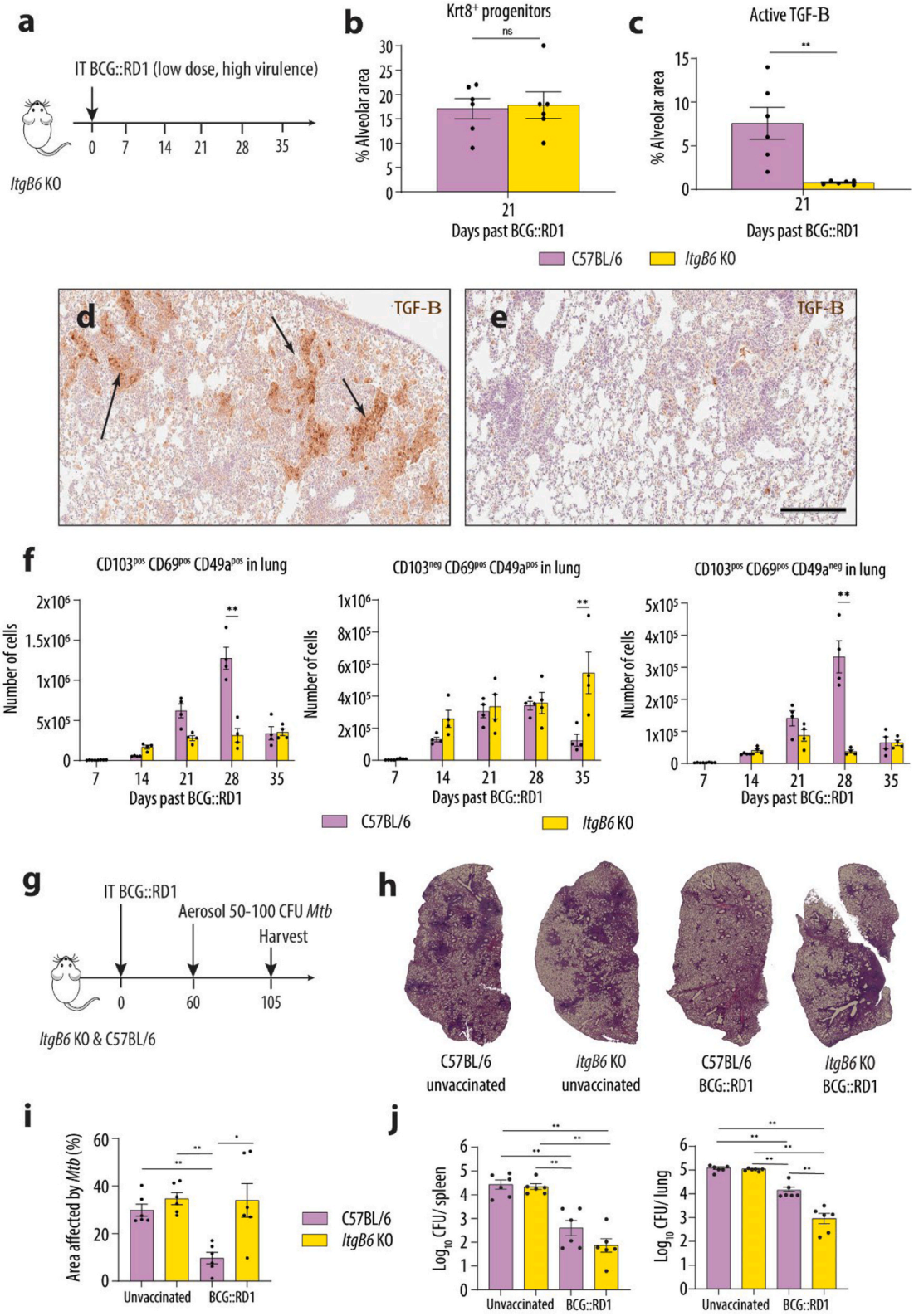

Fig. 8. ***Itgβ6 KO*** **mice demonstrate significantly decreased numbers of CD8$^+$ T$_{RM}$ following mucosal BCG::RD1 vaccination. a)** Experimental design for *Itgβ6 KO* experiments. **b)** Quantification of Krt8$^+$ TP in *Itgβ6 KO* mice at 21 days after BCG::RD1vaccination. **c)** Quantification of extracellular interstitial expression (**d**-arrows) of active TGF-β in alveolar tissue of **d)** C57BL/6 and **e)** *ItgB6 KO* mice 21 days after IT BCG::RD1 vaccination. **f)** Flow cytometry quantification of numbers of CD8$^+$ T$_{RM}$ subsets from day 7–35 after BCG::RD1 vaccination. **g)** Experimental design for *Mtb* challenge experiments. **h)** Histology and quantification of area of lung affected by *Mtb* in naïve (unvaccinated), C57BL/6 wild type and *Itgβ6 KO* BCG::RD1 vaccinated mice at 45 days after *Mtb* challenge and 105 days after BCG::RD1 vaccination. **i)** Individual $\log_{10}$ CFU counts per spleen and lung at day 45 past aerosol challenge with *Mtb*. Pooled data from two independent experiments where n = 6–10 for each timepoint. **f**) $^*P < 0.05$; $^{**}P < 0.01$ by unpaired Student's *t* test. **i, j)** $^{**}P < 0.01$ by Mann Whitney *U* test. **d, e)** Magnification, 10×; Scale bar 200 μm.

lungs, our results add further evidence that CD8$^+$ T_{RM} have a distinctive *lack* of endurance in the lungs,[75] compared to other tissues, which is thought to be organ specific.[20,52,76] Our findings support that mucosally delivered BCG led to robust induction of lung CD8$^+$ T_{RM} which persisted for up to 4 months, albeit numbers waned across the timeline of each of the vaccinations. Therefore, although the virulence and dose of mucosal BCG induced greater numbers of lung CD8$^+$ T_{RM}, they did not improve T_{RM} persistence in the lungs. It is intuitive that over the lifespan of a human whose lungs encounter a myriad of respiratory pathogens, numerous depots of accumulative parenchymal CD8$^+$ T_{RM} could be deleterious for the delicate architecture and surface area required for efficient gas exchange. Undeniably, lung CD8$^+$ T_{RM} have unique organ-specific mechanisms for maturation, persistence, and egress.[77]

We demonstrated the importance of the early resolution of inflammation and downregulation of TGF-β following mucosal BCG vaccination, as this corresponds to the turning point for lung regeneration.[78] We learned that excessive AEC losses mobilised distal airway epithelial progenitors and this was found to relate to TGF-β activation in bronchiolar epithelium and alveolar interstitium. Although this may have resulted in more CD8$^+$ T_{RM}, increased levels or time of activated TGF-β was also shown to harm the lungs. Therefore, an optimal pulmonary mucosal vaccine should enhance local epithelial progenitor responses and keep interstitial active TGF-β levels low so as not to tip the balance between CD8$^+$ T_{RM} induction and tissue integrity.[56,58,78–82] We will continue dose-escalation studies in mice using mucosally delivered BCG, to ameliorate severity of lung pathology linked to excessive levels of active TGF-β and determine an optimal dose-range for protection against secondary *Mtb* challenge.

Ours is the first study to demonstrate the importance of the role of Krt8$^+$ TP to lung restitution following mucosal BCG vaccination. We did not observe development of chronic lesions following any of the three IT vaccinations with BCG, bar in the *Axin2$^{CreERT:TdT}$/EYFP* mice after BCG::RD1 vaccination. At 120 days after IT BCG vaccination, we observed that in the C57BL/6, *Sox2^{CreERT2}/Ai14*, and *Krt5^{CreERT2}* mice, the epithelial progenitors that responded after injury successfully underwent transition from the Sox2$^+$ distal airway and pSPC$^+$ alveolar phenotype through the Krt8$^+$ TP state and on into differentiation into AEC1 evidenced by overall lung restitution. This implies that the TGF-β signaling necessary for early upregulation of *Krt8* and therefore induction of the Krt8$^+$ TP state was appropriate while subsequent inactivation of TGF-β promoted terminal differentiation into AEC1.[83] While out of the scope of this research, in the future the IT BCG vaccinations employed here may be of use to characterize the pathways that induce the Krt8$^+$ transitional state and those that abnormally maintain it that are said to cause chronic lung disease and failure.[84,85]

In fact, pulmonary biologists describe the Krt5$^+$ CD8$^+$ T_{RM} pods (aka RAMD) that form following severe influenza infection as dysplastic.[86,87] We also observed Krt5$^+$ cells in the centre of dysplastic lung lesions in the *Axin2$^{CreERT:TdT}$/EYFP* mice 56 and 120 days after vaccination with BCG::RD1. We suggest that DASC were mobilised in these animals due to the severity of lung injury; this notion is supported by human explant and autopsy studies of lung tissue following SARS-CoV-2 infection in which non-resolvable chronic lung lesions resulted in the recruitment of KRT5$^+$ cells adjacent to fibrotic areas of lung long after clearance of infectious virus.[24,25,88]

Perhaps the most valuable finding of the study was the evidence of cells with CD8$^+$ T_{RM} phenotypes in the lung-draining mLN. It was originally thought that CD8$^+$ T_{RM} were terminally differentiated, permanent residents of the non-lymphoid tissue in which they develop, however, studies have shown that they retain developmental plasticity and have the capacity to recirculate in blood, lymph, and rehome to non-lymphoid tissues (including the tissue of their origin). Studies using *in situ* antigen stimulation via peptide challenge have demonstrated that secondary antigen exposure of T_{RM} at barrier non-lymphoid sites can cause progeny T_{RM} to gain access to draining lymph nodes leading to abundant numbers of antigen-specific CD8$^+$ T_{RM} in draining lymph nodes.[89–91] As lung CD8$^+$ T_{RM} are known to egress to the lung-draining mLN, our findings of cells with CD8$^+$ T_{RM} phenotypes in the mLN may have important significance for an anti-TB vaccine strategy. For example, the cells that we describe in the mLN with the CD103$^-$CD69$^+$CD49a$^+$ T_{RM} phenotype are said to have the capacity to repopulate the lungs as T_{RM} following secondary infection.[92–94] Our future studies will investigate the function of these BCG antigen-specific mLN T_{RM} in mediation of immunity to secondary *Mtb* infection and determine whether they can be exploited as a regional anti-TB arsenal for the lungs.

CRediT authorship contribution statement

Judith A. Blake: Writing – review & editing, Writing – original draft, Visualization, Methodology, Investigation, Formal analysis, Data curation, Conceptualization. **Julia Seifert:** Investigation. **Socorro Miranda-Hernandez:** Visualization, Investigation, Formal analysis. **Roland Ruscher:** Methodology. **Paul R. Giacomin:** Writing – review & editing, Formal analysis, Conceptualization. **Denise L. Doolan:** Writing – review & editing, Formal analysis, Conceptualization. **Andreas Kupz:** Writing – review & editing, Writing – original draft, Supervision, Methodology, Investigation, Funding acquisition, Formal analysis, Conceptualization.

Funding

This work was supported by the National Health and Medical Research Council of Australia (NHMRC) via an Investigator grant (GNT2008715) and an Ideas grant GNT2001262 to A.K.; and a James Cook University Prestige Scholarship to J.A.B.

Declaration of competing interest

The authors declare that they have no known competing financial interests or personal relationships that could have appeared to influence the work reported in this paper.

Acknowledgments

We thank M. Stafford and J. Whan for technical assistance; F. Davis, E. Morrisey, D. Sheppard, S. Mueller for generously sharing mouse lines; University of Queensland Genetic Research Services for genotyping animals and Developmental Studies Hybridoma Bank for reagents.

Appendix A. Supplementary data

Supplementary data to this article can be found online at https://doi.org/10.1016/j.mucimm.2025.05.007.

References

1. Kaufmann SH. Tuberculosis vaccines: time to think about the next generation. *Semin Immunol*. 2013;25(2):172–181.
2. World Health Organisation. *Global tuberculosis report 2024*. World Health Organisation; 2024.
3. Gengenbacher M, Nieuwenhuizen NE, Kaufmann S. BCG - old workhorse, new skills. *Curr Opin Immunol*. 2017;47:8–16.
4. Kaufmann SH, Lange C, Rao M, et al. Progress in tuberculosis vaccine development and host-directed therapies–a state of the art review. *Lancet Respir Med*. 2014;2(4):301–320.
5. Mangtani P, Abubakar I, Ariti C, et al. Protection by BCG vaccine against tuberculosis: a systematic review of randomized controlled trials. *Clin Infect Dis*. 2014;58(4):470–480.
6. Mangtani P, Nguipdop-Djomo P, Keogh RH, et al. Observational study to estimate the changes in the effectiveness of bacillus calmette-guerin (BCG) vaccination with time since vaccination for preventing tuberculosis in the UK. *Health Technol Assess*. 2017;21(39):1–54.
7. Pym AS, Brodin P, Brosch R, Huerre M, Cole ST. Loss of RD1 contributed to the attenuation of the live tuberculosis vaccines Mycobacterium bovis BCG and Mycobacterium microti. *Mol Microbiol*. 2002;46(3):709–717.

8. Aguilo N, Gonzalo-Asensio J, Alvarez-Arguedas S, et al. Reactogenicity to major tuberculosis antigens absent in BCG is linked to improved protection against Mycobacterium tuberculosis. *Nat Commun*. 2017;8:16085.
9. Hsu T, Hingley-Wilson SM, Chen B, et al. The primary mechanism of attenuation of bacillus Calmette-Guerin is a loss of secreted lytic function required for invasion of lung interstitial tissue. *Proc Natl Acad Sci U S A*. 2003;100(21):12420–12425.
10. Perdomo C, Zedler U, Kuhl AA, et al. Mucosal BCG vaccination induces protective lung-resident memory T cell populations against Tuberculosis. *MBio*. 2016;7(6).
11. Muruganandah V, Sathkumara HD, Pai S, et al. A systematic approach to simultaneously evaluate safety, immunogenicity, and efficacy of novel tuberculosis vaccination strategies. *Sci Adv*. 2020;6(10), eaaz1767.
12. Sathkumara HD, Muruganandah V, Cooper MM, et al. Mucosal delivery of ESX-1-expressing BCG strains provides superior immunity against tuberculosis in murine type 2 diabetes. *Proc Natl Acad Sci U S A*. 2020;117(34):20848–20859.
13. Atladottir HO, Thorsen P, Ostergaard L, et al. Maternal infection requiring hospitalization during pregnancy and autism spectrum disorders. *J Autism Dev Disord*. 2010;40(12):1423–1430.
14. Alvarado AG, Lathia JD. Taking a toll on self-renewal: TLR-mediated innate immune signaling in stem cells. *Trends Neurosci*. 2016;39(7):463–471.
15. Agudo J, Park ES, Rose SA, et al. Quiescent tissue stem cells evade immune surveillance. *Immunity*. 2018;48(2):271–285 e275.
16. Ordovas-Montanes J, Dwyer DF, Nyquist SK, et al. Allergic inflammatory memory in human respiratory epithelial progenitor cells. *Nature*. 2018;560(7720):649–654.
17. Belkaid Y, Hand TW. Role of the microbiota in immunity and inflammation. *Cell*. 2014;157(1):121–141.
18. Rieder F, Brenmoehl J, Leeb S, Scholmerich J, Rogler G. Wound healing and fibrosis in intestinal disease. *Gut*. 2007;56(1):130–139.
19. Kumar PA, Hu Y, Yamamoto Y, et al. Distal airway stem cells yield alveoli in vitro and during lung regeneration following H1N1 influenza infection. *Cell*. 2011;147(3):525–538.
20. Takamura S. Persistence in Temporary lung niches: a survival strategy of lung-resident memory CD8(+) T cells. *Viral Immunol*. 2017;30(6):438–450.
21. Vaughan AE, Brumwell AN, Xi Y, et al. Lineage-negative progenitors mobilize to regenerate lung epithelium after major injury. *Nature*. 2015;517(7536):621–625.
22. Zacharias WJ, Frank DB, Zepp JA, et al. Regeneration of the lung alveolus by an evolutionarily conserved epithelial progenitor. *Nature*. 2018;555(7695):251–255.
23. Chua RL, Lukassen S, Trump S, et al. COVID-19 severity correlates with airway epithelium-immune cell interactions identified by single-cell analysis. *Nat Biotechnol*. 2020;38(8):970–979.
24. Fang Y, Liu H, Huang H, et al. Distinct stem/progenitor cells proliferate to regenerate the trachea, intrapulmonary airways and alveoli in COVID-19 patients. *Cell Res*. 2020;30(8):705–707.
25. Jyothula SSK, Peters A, Liang Y, et al. Fulminant lung fibrosis in non-resolvable COVID-19 requiring transplantation. *EBioMedicine*. 2022;86, 104351.
26. Zhao Z, Zhao Y, Zhou Y, Wang X, Zhang T, Zuo W. Single-cell analysis identified lung progenitor cells in COVID-19 patients. *Cell Prolif*. 2020;53(12), e12931.
27. Takamura S, Yagi H, Hakata Y, et al. Specific niches for lung-resident memory CD8+ T cells at the site of tissue regeneration enable CD69-independent maintenance. *J Exp Med*. 2016;213(13):3057–3073.
28. Desai TJ, Brownfield DG, Krasnow MA. Alveolar progenitor and stem cells in lung development, renewal and cancer. *Nature*. 2014;507(7491):190–194.
29. Nabhan AN, Brownfield DG, Harbury PB, Krasnow MA, Desai TJ. Single-cell wnt signaling niches maintain stemness of alveolar type 2 cells. *Science*. 2018;359(6380):1118–1123.
30. Ray S, Chiba N, Yao C, et al. Rare SOX2(+) airway progenitor cells generate KRT5(+) cells that repopulate damaged Alveolar Parenchyma following influenza virus infection. *Stem Cell Rep*. 2016;7(5):817–825.
31. Kathiriya JJ, Brumwell AN, Jackson JR, Tang X, Chapman HA. Distinct airway epithelial stem cells Hide among Club cells but mobilize to promote Alveolar regeneration. *Cell Stem Cell*. 2020.
32. Strunz M, Simon LM, Ansari M, et al. Alveolar regeneration through a Krt8+ transitional stem cell state that persists in human lung fibrosis. *Nat Commun*. 2020;11(1):3559.
33. Quantius J, Schmoldt C, Vazquez-Armendariz AI, et al. Influenza virus infects epithelial stem/progenitor cells of the distal lung: impact on Fgfr2b-driven epithelial repair. *PLoS Pathog*. 2016;12(6), e1005544.
34. Takamura S. Niches for the long-term maintenance of tissue-resident memory T cells. *Front Immunol*. 2018;9:1214.
35. Choi J, Park JE, Tsagkogeorga G, et al. Inflammatory signals induce AT2 cell-derived damage-associated transient progenitors that mediate Alveolar regeneration. *Cell Stem Cell*. 2020;27(3):366–382 e367.
36. Kobayashi Y, Tata A, Konkimalla A, et al. Persistence of a regeneration-associated, transitional alveolar epithelial cell state in pulmonary fibrosis. *Nat Cell Biol*. 2020;22(8):934–946.
37. Dhakal S, Park HS, Seddu K, et al. Estradiol mediates greater germinal center responses to influenza vaccination in female than male mice. *MBio*. 2024;15(4), e0032624.
38. Ursin RL, Dhakal S, Liu H, et al. Greater breadth of vaccine-induced immunity in females than males is mediated by increased antibody diversity in germinal center B cells. *MBio*. 2022;13(4), e0183922.
39. Chuquimia OD, Petursdottir DH, Rahman MJ, Hartl K, Singh M, Fernandez C. The role of alveolar epithelial cells in initiating and shaping pulmonary immune responses: communication between innate and adaptive immune systems. *PLoS One*. 2012;7(2), e32125.
40. Whitsett JA, Weaver TE. Alveolar development and disease. *Am J Respir Cell Mol Biol*. 2015;53(1):1–7.
41. Fedchenko N, Reifenrath J. Different approaches for interpretation and reporting of immunohistochemistry analysis results in the bone tissue - a review. *Diagn Pathol*. 2014;9:221.
42. Nonneoplastic Lesion Atlas - National Toxicology Program (Respiratory System). https://ntp.niehs.nih.gov/atlas/nnl/respiratory-system, 2021, Accessed Date Accessed 2021 Accessed.
43. Zareba L, Piszczatowska K, Dzaman K, et al. The relationship between fine Particle matter (PM2.5) exposure and upper respiratory Tract diseases. *J Pers Med*. 2024;14(1).
44. Muzumdar MD, Tasic B, Miyamichi K, Li L, Luo L. A global double-fluorescent cre reporter mouse. *Genesis*. 2007;45(9):593–605.
45. Zuo W, Zhang T, Wu DZ, et al. p63(+)Krt5(+) distal airway stem cells are essential for lung regeneration. *Nature*. 2015;517(7536):616–620.
46. Topham DJ, Reilly EC, Emo KL, Sportiello M. Formation and maintenance of tissue resident memory CD8+ T cells after viral infection. *Pathogens*. 2019;8(4).
47. Eriksson M, Nylen S, Gronvik KO. T cell kinetics reveal expansion of distinct lung T cell subsets in acute versus in resolved influenza virus infection. *Front Immunol*. 2022;13, 949299.
48. Hayward SL, Scharer CD, Cartwright EK, et al. Environmental cues regulate epigenetic reprogramming of airway-resident memory CD8(+) T cells. *Nat Immunol*. 2020;21(3):309–320.
49. Hogan RJ, Usherwood EJ, Zhong W, et al. Activated antigen-specific CD8+ T cells persist in the lungs following recovery from respiratory virus infections. *J Immunol*. 2001;166(3):1813–1822.
50. Slutter B, Van Braeckel-Budimir N, Abboud G, Varga SM, Salek-Ardakani S, Harty JT. Dynamics of influenza-induced lung-resident memory T cells underlie waning heterosubtypic immunity. *Sci Immunol*. 2017;2(7).
51. Wu T, Hu Y, Lee YT, et al. Lung-resident memory CD8 T cells (TRM) are indispensable for optimal cross-protection against pulmonary virus infection. *J Leukoc Biol*. 2014;95(2):215–224.
52. Carbone FR. Unique properties of tissue-resident memory T cells in the lungs: implications for COVID-19 and other respiratory diseases. *Nat Rev Immunol*. 2023;23(5):329–335.
53. Takamura S, Kohlmeier JE. Establishment and maintenance of conventional and circulation-driven lung-resident memory CD8(+) T cells following respiratory virus infections. *Front Immunol*. 2019;10:733.
54. Mackay LK, Rahimpour A, Ma JZ, et al. The developmental pathway for CD103(+) CD8+ tissue-resident memory T cells of skin. *Nat Immunol*. 2013;14(12):1294–1301.
55. Nath AP, Braun A, Ritchie SC, et al. Comparative analysis reveals a role for TGF-beta in shaping the residency-related transcriptional signature in tissue-resident memory CD8+ T cells. *PLoS One*. 2019;14(2), e0210495.
56. Munger JS, Huang X, Kawakatsu H, et al. The integrin alpha v beta 6 binds and activates latent TGF beta 1: a mechanism for regulating pulmonary inflammation and fibrosis. *Cell*. 1999;96(3):319–328.
57. Chapman HA, Li X, Alexander JP, et al. Integrin alpha6beta4 identifies an adult distal lung epithelial population with regenerative potential in mice. *J Clin Invest*. 2011;121(7):2855–2862.
58. Auyeung VC, Downey MS, Thamsen M, et al. IRE1alpha drives lung epithelial progenitor dysfunction to establish a niche for pulmonary fibrosis. *Am J Physiol Lung Cell Mol Physiol*. 2022;322(4):L564–L580.
59. Topham DJ, Reilly EC. Tissue-resident memory CD8(+) T cells: from phenotype to function. *Front Immunol*. 2018;9:515.
60. Sheppard D. Transforming growth factor beta: a central modulator of pulmonary and airway inflammation and fibrosis. *Proc Am Thorac Soc*. 2006;3(5):413–417.
61. Peng ZW, Ikenaga N, Liu SB, et al. Integrin alphavbeta6 critically regulates hepatic progenitor cell function and promotes ductular reaction, fibrosis, and tumorigenesis. *Hepatology*. 2016;63(1):217–232.
62. Munger JS, Sheppard D. Cross talk among TGF-beta signaling pathways, integrins, and the extracellular matrix. *Cold Spring Harb Perspect Biol*. 2011;3(11), a005017.
63. Casey KA, Fraser KA, Schenkel JM, et al. Antigen-independent differentiation and maintenance of effector-like resident memory T cells in tissues. *J Immunol*. 2012;188(10):4866–4875.
64. Sallusto F, Geginat J, Lanzavecchia A. Central memory and effector memory T cell subsets: function, generation, and maintenance. *Annu Rev Immunol*. 2004;22:745–763.
65. Meliopoulos VA, Van de Velde LA, Van de Velde NC, et al. An epithelial integrin regulates the amplitude of protective lung interferon responses against multiple respiratory pathogens. *PLoS Pathog*. 2016;12(8), e1005804.
66. Meliopoulos V, Livingston B, Van de Velde LA, Honce R, Schultz-Cherry S. Absence of beta6 integrin reduces influenza disease severity in highly Susceptible obese mice. *J Virol*. 2019;93(2).
67. O'Garra A, Redford PS, McNab FW, Bloom CI, Wilkinson RJ, Berry MP. The immune response in tuberculosis. *Annu Rev Immunol*. 2013;31:475–527.
68. Nunes-Alves C, Booty MG, Carpenter SM, Jayaraman P, Rothchild AC, Behar SM. In search of a new paradigm for protective immunity to TB. *Nat Rev Microbiol*. 2014;12(4):289–299.
69. Simonson AW, Zeppa JJ, Bucsan AN, et al. Intravenous BCG-mediated protection against tuberculosis requires CD4+ T cells and CD8alpha+ lymphocytes. *J Exp Med*. 2025;222(4).
70. Ernst JD. The immunological life cycle of tuberculosis. *Nat Rev Immunol*. 2012;12(8):581–591.
71. Cooper AM, Torrado E. Protection versus pathology in tuberculosis: recent insights. *Curr Opin Immunol*. 2012;24(4):431–437.
72. Sharpe S, White A, Sarfas C, et al. Alternative BCG delivery strategies improve protection against Mycobacterium tuberculosis in non-human primates: protection

associated with mycobacterial antigen-specific CD4 effector memory T-cell populations. *Tuberculosis (Edinb)*. 2016;101:174–190.
73. Uranga S, Marinova D, Martin C, Aguilo N. Protective efficacy and Pulmonary immune response following subcutaneous and intranasal BCG Administration in Mice. *J Vis Exp*. 2016;115.
74. Satti I, Marshall JL, Harris SA, et al. Safety of a controlled human infection model of tuberculosis with aerosolised, live-attenuated Mycobacterium bovis BCG versus intradermal BCG in BCG-naive adults in the UK: a dose-escalation, randomised, controlled, phase 1 trial. *Lancet Infect Dis*. 2024;24(8):909–921.
75. Ogongo P, Porterfield JZ, Leslie A. Lung tissue resident memory T-cells in the immune response to Mycobacterium tuberculosis. *Front Immunol*. 2019;10:992.
76. Stolley JM, Masopust D. Tissue-resident memory T cells live off the fat of the land. *Cell Res*. 2017;27(7):847–848.
77. Mackay LK, Wynne-Jones E, Freestone D, et al. T-box transcription factors combine with the cytokines TGF-beta and IL-15 to control tissue-resident memory T cell fate. *Immunity*. 2015;43(6):1101–1111.
78. Kim KK, Sheppard D, Chapman HA. TGF-beta1 signaling and tissue fibrosis. *Cold Spring Harb Perspect Biol*. 2018;10(4).
79. Jenkins RG, Su X, Su G, et al. Ligation of protease-activated receptor 1 enhances alpha(v)beta6 integrin-dependent TGF-beta activation and promotes acute lung injury. *J Clin Invest*. 2006;116(6):1606–1614.
80. Pittet JF, Griffiths MJ, Geiser T, et al. TGF-beta is a critical mediator of acute lung injury. *J Clin Invest*. 2001;107(12):1537–1544.
81. Riemondy KA, Jansing NL, Jiang P, et al. Single cell RNA sequencing identifies TGFbeta as a key regenerative cue following LPS-induced lung injury. *JCI Insight*. 2019;5(8).
82. Khalil N, Parekh TV, O'Connor R, et al. Regulation of the effects of TGF-beta 1 by activation of latent TGF-beta 1 and differential expression of TGF-beta receptors (T beta R-I and T beta R-II) in idiopathic pulmonary fibrosis. *Thorax*. 2001;56(12):907–915.
83. Jiang P, Gil de Rubio R, Hrycaj SM, et al. Ineffectual type 2-to-type 1 Alveolar epithelial cell differentiation in idiopathic Pulmonary fibrosis: persistence of the KRT8(hi) transitional state. *Am J Respir Crit Care Med*. 2020;201(11):1443–1447.
84. Yao C, Guan X, Carraro G, et al. Senescence of Alveolar type 2 cells drives progressive Pulmonary fibrosis. *Am J Respir Crit Care Med*. 2021;203(6):707–717.
85. Narasimhan H, Cheon IS, Qian W, et al. Proximal immune-epithelial progenitor interactions drive chronic tissue sequelae post COVID-19. *Res Sq*. 2023.
86. Planer JD, Morrisey EE. After the storm: regeneration, repair, and reestablishment of homeostasis between the Alveolar epithelium and innate immune system following viral lung injury. *Annu Rev Pathol*. 2023;18:337–359.
87. de Mello F, Costa M, Weiner AI, Vaughan AE. Basal-like progenitor cells: a review of dysplastic Alveolar regeneration and remodeling in lung repair. *Stem Cell Rep*. 2020;15(5):1015–1025.
88. Wu K, Zhang Y, Austin SR, Declue HY, Byers DE, Crouch EC *et al.* Lung remodeling regions in long-term Covid-19 feature basal epithelial cell reprogramming. *medRxiv* 2022.
89. Beura LK, Wijeyesinghe S, Thompson EA, et al. T cells in nonlymphoid tissues give rise to lymph-node-resident memory T cells. *Immunity*. 2018;48(2):327–338 e325.
90. Stolley JM, Johnston TS, Soerens AG, et al. Retrograde migration supplies resident memory T cells to lung-draining LN after influenza infection. *J Exp Med*. 2020;217(8).
91. Fonseca R, Beura LK, Quarnstrom CF, et al. Developmental plasticity allows outside-in immune responses by resident memory T cells. *Nat Immunol*. 2020;21(4):412–421.
92. Christo SN, Evrard M, Park SL, et al. Discrete tissue microenvironments instruct diversity in resident memory T cell function and plasticity. *Nat Immunol*. 2021;22(9):1140–1151.
93. Paik DH, Farber DL. Influenza infection fortifies local lymph nodes to promote lung-resident heterosubtypic immunity. *J Exp Med*. 2021;218(1).
94. Brewitz A, Eickhoff S, Dahling S, et al. CD8(+) T cells orchestrate pDC-XCR1(+) dendritic cell spatial and functional cooperativity to optimize priming. *Immunity*. 2017;46(2):205–219.